Pattern selection in extended periodically forced systems: A continuum coupled map approach

Shankar C. Venkataramani*
Department of Mathematics, University of Chicago, Chicago, Illinois 60637

Edward Ott
Department of Physics, University of Maryland, College Park, Maryland 20742
(Received 23 June 2000; published 20 March 2001)

We propose that a useful approach to the modeling of periodically forced extended systems is through continuum coupled map (CCM) models. CCM models are discrete time, continuous space models, mapping a continuous spatially varying field $\xi_n(\mathbf{x})$ from time n to time $n+1$. The efficacy of CCM models is illustrated by an application to experiments of Umbanhowar, Melo, and Swinney [Nature **382**, 793 (1996)] on vertically vibrated granular layers. Using a simple CCM model incorporating temporal period doubling and spatial patterning at a preferred length scale, we obtain results that bear remarkable similarities to the experimental observations. The fact that the model does not make use of physics specific to granular layers suggests that similar phenomena may be observed in other (nongranular) periodically forced, strongly dissipative systems. We also present a framework for the analysis of pattern selection in CCM models using a truncated modal expansion. Through the analysis, we predict scaling laws of various quantities, and these laws may be verifiable experimentally.

DOI: 10.1103/PhysRevE.63.046202 PACS number(s): 45.70.Qj, 05.65.+b, 45.70.−n, 05.45.−a

I. INTRODUCTION

Pattern formation is a ubiquitous phenomenon in the dynamics of extended nonlinear systems [1,2]. A few examples of pattern forming systems are coupled reaction-diffusion systems [3], vertically vibrated fluids (Faraday waves) [4], Rayleigh-Bénard convection [5], and heart tissue [6]. Patterns in extended systems arise as a result of the interplay of many factors, including the external forcing and/or the excitable nature of the medium, the spatial interactions between the different parts of the extended system, and internal dissipation. It is often the case that exact dynamical equations for these systems cannot be determined. Furthermore, even if exact equations and parameters are determined, the equations are often very hard to solve. Therefore, a useful approach to studying the dynamics of extended nonlinear systems is through the formulation of generic models.

Generic models (or model equations) are dynamical equations that are much simpler than exact equations for the system of interest. However, they are designed to include key features of the exact equations that are suspected to lead to qualitative phenomena seen in real systems (e.g., pattern formation [1], coherent states and solitary waves [7], bifurcations, spatiotemporal chaos [8], nontrivial collective behavior [9], etc.). These models are therefore very useful in exposing the typical behavior to be expected in nonlinear pattern forming extended systems. Examples of such models include the Swift-Hohenberg equation, the complex Ginzburg-Landau equation, and the Kuromoto-Shivashinsky equation.

There are various classes of generic models including partial differential equations (PDE models), lattices of ordinary differential equations (LODE models), coupled map lattices (CML models), and cellular automata (CA models). These classes of models are be distinguished by whether they choose to treat the time, space, and field variables as continuous or discrete. This is illustrated in Table I, where we also list a previously rarely used model class, which we call continuum coupled map (CCM) models. In particular, CCMs are discrete time, continuous space models, that map a continuous field variable defined on a continuous spatial domain forward from a discrete time index n to time index $n+1$. Therefore, a CCM model is specified by giving an operator $\mathcal{F}[\cdot]$, that maps the continuous field $\xi_n(\mathbf{x})$ forward in time:

$$\xi_{n+1}(\mathbf{x}) = \mathcal{F}[\xi_n(\mathbf{x})].$$

CCM models are particularly well suited for the study of periodically forced extended systems for the following reasons.

(1) Because of the periodic forcing, the system does not have a continuous time translation symmetry. Rather, it has a discrete time translation symmetry for translations by multiples of the forcing period. Therefore, a map is particularly appropriate for modeling the temporal dynamics of the system.

(2) Using a continuous field on a continuous spatial domain enables one to model patterns unconstrained by an imposed grid. This is appropriate for the modeling of patterns in extended systems.

(3) Since the temporal dynamics are given by a map, and we can efficiently implement spatial coupling operators by spectral (fast Fourier transform) techniques, numerical implementations of CCM models can be made very efficient. This makes it possible to run simulations of CCM models much longer than simulations of equivalent PDE models for the same computational effort.

*Electronic address: shankar@math.uchicago.edu

TABLE I. Classes of models for the description of pattern forming systems. The other possible classes (discrete field variable and a continuous spatial domain or time) appear not to be physically relevant, since the dynamics is either discontinuous in space or time, or is trivial.

Model type	Field variable(s)	Spatial domain	Time
PDE	Continuous	Continuous	Continuous
LODE	Continuous	Discrete	Continuous
CML	Continuous	Discrete	Discrete
CA	Discrete	Discrete	Discrete
CCM	Continuous	Continuous	Discrete

In this paper, we will use a CCM model to examine the consequences of the interaction between temporal period doubling and spatial pattern formation with a preferred length scale. This work was originally motivated by experiments [10–12] in which the authors observed the formation of a variety of two-dimensional patterns in a vertically vibrated thin granular layer [13]. We will see that the CCM approach is very fruitful for the consideration of these experiments.

This paper is organized as follows: In Sec. II, we briefly review the recent experimental results [10–12] and the experimental phase diagram. In Sec. III, we discuss some of the theoretical approaches to modeling these experiments. In Sec. IV, we give some motivation for the CCM model equations that we propose for describing the experiment. In Sec. V, we present results from numerical simulations of our model and compare these results with the experimental observations. We present a summary of the results of our analysis of the pattern formation in Sec. VI. In Secs. VII–IX, we give a detailed account of the analysis and we present a concluding discussion in Sec. X.

II. VIBRATED GRANULAR LAYERS

In the experiments in Refs. [10–12], the granular layer consists of brass spheres, is supported from below by a horizontal plate, and has an upper free surface. The system is driven by vertically vibrating the plate sinusoidally. Varying the amplitude A and the frequency f_0 of the sinusoidal vibration leads to the formation of, and transitions between various patterned states. These patterns are roughly analogous to Faraday wave patterns in vibrated liquid layers.

A variety of patterns are seen in these experiments. For example, in Ref. [10], holding f_0 fixed and increasing the oscillation amplitude, the following sequence of states was observed: a uniform flat state oscillating at f_0; a stripe pattern oscillating at $f_0/2$ (i.e., the period of the pattern oscillation is double the vibrational period); a hexagonal pattern, also at $f_0/2$; two flat domains separated by a ''kink'' with each domain oscillating at $f_0/2$ but with each in one of the two possible temporal $f_0/2$ phases of oscillation; competing square and stripe patterns at $f_0/4$ (i.e., a further period doubling has occurred); $f_0/4$ hexagonal patterns; and, at higher driving, patterns disordered in space and time. (See Figs. 1(a)–1(f) of Ref. [10].)

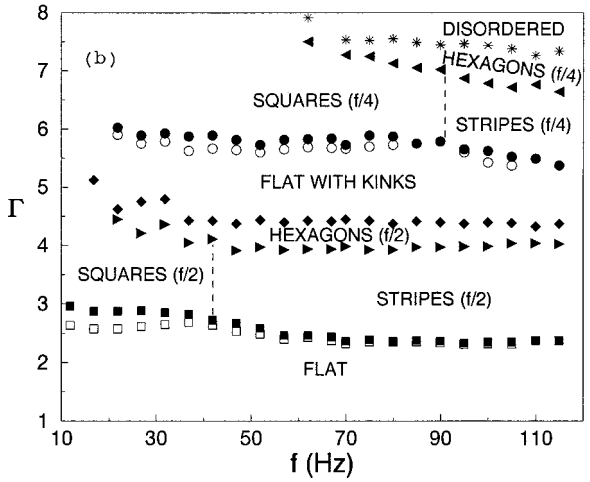

FIG. 1. Experimental phase diagram from Refs. [10,12].

Figure 1 shows an experimental phase diagram from Ref. [10], where Γ is the nondimensionalized oscillation amplitude:

$$\Gamma = (2\pi f_0)^2 A/g.$$

Here A is the amplitude of the oscillation of the plate, f_0 is the oscillation frequency, and g is the acceleration of gravity.

The results in Fig. 1 were obtained for a relatively thin layer, about seven grain diameters thick. When the layer thickness is increased (e.g., to 15 diameters) additional phenomena are observed. These patterns were reported in Refs. [11] and [12]. The most interesting of these additional phenomena is the presence of localized, solitary structures oscillating at $f_0/2$, which the authors called *oscillons*. An oscillon is a long-lived localized $f_0/2$ structure that exists as an alternation between a hill and a depression of the layer surface. These oscillons can be isolated (i.e., surrounded by the f_0 flat state), or else can exist in bound states of two, three, or more regularly arranged oscillons. The oscillon phenomenon is observed in the vicinity of the transition between the f_0 flat state and the $f_0/2$ patterns.

III. MODELING GRANULAR FLOWS

As the authors remarked in Ref. [12], these experiments provide a challenge to theory. In the case of Faraday waves, that is, parametrically driven surface waves in vibrated liquid layers, the Navier-Stokes equations give a complete description of the dynamics of the system. The onset criteria for the patterns can be derived from these equations, both for ideal fluids [14] and for viscous fluids [15]. The Navier-Stokes equations can also be reduced to amplitude equations [16], that provide a good description of the pattern formation in Faraday waves. The situation is very different for granular flows. For granular flows, there exist no equations, that correspond in stature and in the range of applicability, to the Navier-Stokes equations for fluids [17,18]. It is therefore a challenge to build an analytical model of the pattern formation seen in vibrated granular layers.

The only direct, first-principles approach to studying the

dynamics of granular materials with many interacting particles has been molecular-dynamics-type numerical simulations. Such molecular dynamics simulations of spheres on a vibrating plate reproduce the experimentally observed phenomena [19] qualitatively and quantitatively. From the measured single particle velocity distributions as well as the correlations of the particle positions and velocities in the simulations [19], the authors concluded that a useful approach to model the granular flows in the experiments [10–12] is through the continuum equations obtained from the kinetic theory of dissipative gases [20]. The results in Ref. [21], which revealed a continuum type stability diagram for the stripe patterns, also suggested that a continuum model will be appropriate for modeling the granular flow in the vibrated layers. In ongoing work, many authors worked on the validation of the continuum equations by comparison with molecular dynamics simulations, as well as using the equations to study the phenomena in vibrated granular layers [22].

Another useful approach to this problem has been to postulate phenomenological equations for the vibrated granular layer based on physical considerations or using analogies with hydrodynamics [23–28]. These models give results that are in qualitative agreement with the experiments in portions of the phase space. However, different models make different assumptions in modeling the underlying physics of the granular flow, or else have undetermined coefficients which are set in order to give agreement with the experiment. Therefore, it is difficult to judge the relevance of the particular physical ideas in these models to the behavior of granular materials.

Our approach is motivated by the current lack of physical understanding of dynamics of granular media [17], and the possibility that there exist no local equations describing granular flow [18]. Thus, in building our model, we will consider the underlying symmetries of the system and the qualitative features of the dynamics. We will use dimensional analysis to identify the relevant variables, but will strive to avoid modeling the physics of granular flows.

Our model and some of the results from it were first presented in Ref. [29]. The CCM framework arises naturally in our model, since it is particularly suited to the symmetries of the system. To the extent that the model is free of physics specific to the experimental system, we can regard the experimentally observed features reproduced by the model as universal. Although this approach will not shed light on the physics of the underlying granular flow, it will enable us to identify the key dynamical features that lead to the observed experimental behavior.

IV. CCM MODEL FOR VIBRATED GRANULAR LAYERS

Our goal is to produce a phenomenological model of the experimental results and, as stressed above, we wish to use a minimum of physical input in building this model. By this approach, we wish to use our model to test hypotheses concerning the essential model properties necessary for explaining the experimental results. As we argued earlier, the CCM framework is ideal for this task.

It is relevant to consider the dynamics of a single inelastic ball on a vertically vibrated plate, analyzed by Mehta and Luck in Ref. [30]. In this situation, the only control parameter is the nondimensional vibration amplitude $\Gamma = 4\pi^2 f^2 A/g$. Since the ball is inelastic, it loses all its kinetic energy on impact with the plate. On every cycle, the ball lifts off the plate, at the point in the cycle when the acceleration of the plate in the downward direction is greater than the acceleration due to gravity g. In this situation, the ball ''forgets'' its dynamical history in every cycle, and the dynamics can be entirely deduced from a knowledge of the time of flight between one bounce and the next, that is by a one-dimensional map.

This map was analyzed in detail in Ref. [30]. The dynamics for this map is complicated because the map is not smooth (or even continuous). For purposes of our model, the following behaviors, which occur over significant ranges of Γ are the key features of this map.

(1) For $\Gamma > 1$, the ball lifts off the plate at some point in the cycle. The first behavior that is observed is a fixed point for the time of flight map; that is, the dynamics of the ball is the same in every cycle, and the time of flight is shorter than the oscillation period; the ball hits the plate once every cycle.

(2) Increasing Γ above a critical value causes this fixed point to lose stability to a period doubled state. The times of flight alternate between a long flight and a short flight, and these times are such that the ball hits the plate on every oscillation cycle.

(3) Above a larger value of Γ the dynamics of the ball is again given by a fixed point of the time of flight map, but with the time of flight longer than the oscillation period. In this regime, the ball hits the plate only once every two cycles.

These behaviors are represented schematically in Figs. 2(a), 2(b), and 2(c), respectively. Γ is the only relevant dimensionless parameter for the dynamics of a single inelastic ball on a vibrating plate. For a granular layer, the other dimensionless parameters that can be experimentally varied are N, the thickness of the layer in grain diameters, and $\beta = f_0^2 a/g$, which is a dimensionless measure of the frequency of oscillation. Here a is the diameter of a typical grain. The parameter β can be written as a/l, that is as a ratio of two length scales, where $l = g/f_0^2$.

We will first consider the situation where N kept constant, but Γ and β are varied. The first question in formulating a CCM model concerns the dimensionality of the field variable ξ. Obviously the simplest choice is to take the field variable to be a scalar. This is suggested by the fact that the dynamics of a single ball is given by a one-dimensional map. It is also suggested by the very dissipative physics of granular media: when the layer hits the plate its kinetic energy is rapidly dissipated, so that when, later in the cycle, it departs from contact with the plate, it has ''forgotten'' the velocity with which it struck the plate, and one might consequently expect that its subsequent evolution is determined solely by its height profile (a scalar function) at the time it leaves contact with the plate.

The next task is to specify a mapping of ξ from time n to time $n+1$. The basic framework of our CCM model is as

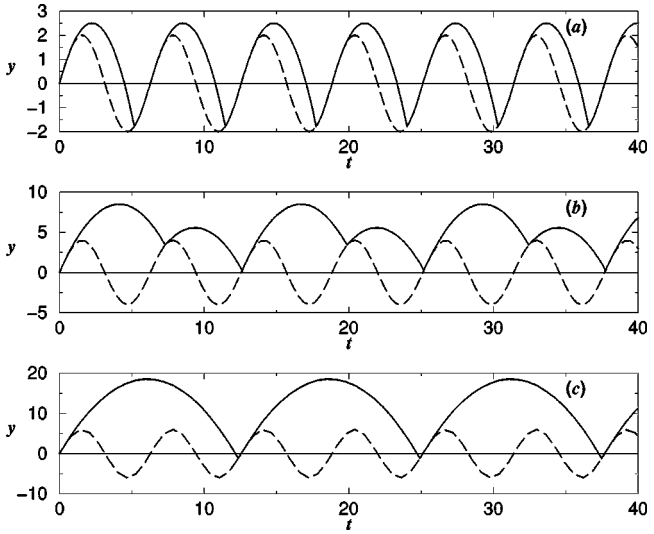

FIG. 2. The various dynamical behaviors of an inelastic ball on a vibrating plate. The solid line depicts the motion of the ball, and the dashed line depicts the motion of the plate. The units along the axes are chosen so that the driving frequency $f_0=1/2\pi$ and the acceleration due to gravity $g=1$. (a) $\Gamma=2$: fixed point for the time of flight map. (b) $\Gamma=4$: period-2 cycle with alternating long and short hops. (c) $\Gamma=6$: fixed point with the ball hitting the plate only once every two cycles.

follows. We consider a scalar field $\xi_n(\mathbf{x})$ at discrete integer valued times n which we think of as roughly representing the height of the granular layer at position $\mathbf{x}$ at a fixed phase of the oscillation cycle. Here $\mathbf{x}$ is a continuous two-dimensional spatial variable. To advance $\xi_n(\mathbf{x})$ forward one time period, we first apply a one-dimensional map M to ξ_n at each point in space,

$$\xi_n'(\mathbf{x})=M[\xi_n(\mathbf{x}),r], \tag{1}$$

where r is a parameter of the chosen map function. Next we augment this nonlinear ''local'' discrete time dynamics with a linear spatial operator $\mathcal{L}$ which couples the dynamics of nearby $\mathbf{x}$ locations:

$$\xi_{n+1}(\mathbf{x})=\mathcal{L}[\xi_n'(\mathbf{x})]. \tag{2}$$

Assuming translational invariance, the operator $\mathcal{L}$ is of the form

$$\mathcal{L}[\xi_n'(\mathbf{x})]=f(\mathbf{x})\otimes\xi_n'(\mathbf{x}), \tag{3}$$

where $\otimes$ denotes convolution. Since we do not expect significant interaction between $\mathbf{x}$ locations that are distant, we require that the spatial coupling function $f(\mathbf{x})$ should decay rapidly for $|\mathbf{x}|\gg\lambda$, for a length scale λ that we will specify below. Letting $\xi_n(\mathbf{k})$ and $\overline{f}(\mathbf{k})$ denote the spatial Fourier transforms of $\xi_n(\mathbf{x})$ and $f(\mathbf{x})$, we have

$$\overline{\xi}_{n+1}(\mathbf{k})=\overline{f}(\mathbf{k})\overline{\xi}_n'(\mathbf{k}). \tag{4}$$

The specification for a CCM model in this framework will consist of choices of the map function M and the function f, specifying the spatial coupling operator $\mathcal{L}$. In Ref. [10] the authors argued that the various patterns they observed are produced by interaction between temporal period doubling and an instability that produces spatial variations on the surface of the layer. We wish to test this in the simplest possible way, using the above CCM framework [Eqs. (1)–(4)]. In particular, in choosing M and f, we use the hypothesis suggested by the experimental results that period doubling and the occurrence of a preferred spatial scale (e.g., the stripe wavelength or the hexagon diameter) are the crucial attributes of this system.

We incorporate the period doubling in the ''local'' temporal dynamics by choosing a unimodal map M that has a period doubling sequence. For most of the numerical results in this paper, we use the map

$$M(\xi,r)=r\exp[-(\xi-1)^2/2]. \tag{5}$$

The map in Eq. (5) is similar to the logistic map $M(\xi,r)=r\xi(1-\xi)$, but it has the advantage that all orbits are bounded. This is in contrast to iterating the logistic map, where an initial negative ξ value yields an orbit $\xi\to-\infty$. One feature of map (5) that will turn out to be relevant to the discussion below is the fact that all the period doublings in this map are supercritical.

Assuming that the ''local'' dynamics in the vibrated granular layer is strongly correlated with the dynamics of a single inelastic ball on a vibrated plate, we are led to identify the model parameter r which controls the ''local'' dynamics in the model with the experimental parameter Γ which controls the dynamics of the single inelastic ball.

The quantity $\gamma=\log|\overline{f}(\mathbf{k})|$ is the growth rate for the amplitude of a perturbation with wave vector $\mathbf{k}$ between two collisions with the plate. Assuming isotropy, we henceforth write $\overline{f}$ as a function of $k=|\mathbf{k}|$. Since $\xi(\mathbf{x})$ is real, $\overline{f}(\mathbf{k})=\overline{f}^*(-\mathbf{k})$, where* denotes complex conjugation. However, since $\overline{f}$ depends only on $|\mathbf{k}|=k$, $\overline{f}(k)$ is real. By the above considerations, at a given forcing frequency f_0, the system has two length scales; a and l. Therefore, the growth rate is of the form

$$\overline{f}(k)=g(k/k_0,k/k_c). \tag{6}$$

We incorporate spatial patterning at a preferred scale k_0^{-1} by taking $|\overline{f}(k)|$ to have a peak at $k=k_0$, with $|\overline{f}(k_0)|>1$. Since the patterns cannot have any structures on scales equal to or smaller than the size of a single grain $|\overline{f}(k)|$ decreases with increasing k, becoming small $[|\overline{f}(k)|\ll1]$ at large k. Finally, we required that $f(\mathbf{x})$ be short ranged, that is $f(\mathbf{x})$ should decay rapidly for $|\mathbf{x}|\gg\lambda$, where λ is the effective range over which the grains interact. Since the particles in the experiment do not move over distances that are large compared to the wavelength of the pattern, an appropriate choice for λ is k_0^{-1}. This implies that $\overline{f}(k)\approx c$ for $k\ll k_0$, for some constant c. Without loss of generality, we can take $c=1$. [If $c\neq1$, we can absorb it by replacing r in Eq. (5) by r/c.]

For simplicity, we choose the product form

$$g(k/k_0,k/k_c)=\phi(k/k_c)\exp[\gamma(k/k_0)]$$

for $g(.,.)$. We satisfy the requirements from above by making the following choices for $\gamma(\cdot)$ and $\phi(\cdot)$

$$\gamma(k)=\frac{1}{2}\left(\frac{k}{k_0}\right)^2\left[1-\frac{1}{2}\left(\frac{k}{k_0}\right)^2\right], \tag{7}$$

$$\phi(k)=\mathrm{sgn}(k_c^2-k^2), \tag{8}$$

where $\mathrm{sgn}(y)=1$ for $y\geqslant 0$ and $\mathrm{sgn}(y)=-1$ for $y<0$.

At $k=0$, we have $\gamma(0)=0$ and $\phi(0)=1$, yielding $\overline{f}(0)=1$. Note that we have chosen γ and ϕ such that $\overline{f}(k)\approx 1$ on scales $k\ll k_0$. Consequently, $f(\mathbf{x})$ looks like a delta function for length scales $|\mathbf{x}|\gg k_0^{-1}$. A consequence of the fact that $\overline{f}(0)=1$ is that the spatially homogeneous states are governed by the map M, and the spatial coupling operator $\mathcal{L}$ does not play a role in the dynamics. Thus, for example, a period doubling of the map M at $r=r_c$ implies the existence of a corresponding transition in the CCM model, namely, a period doubling of the homogeneous state at $r=r_c$.

The form of the growth rate $\gamma(k)=\log|\overline{f}(k)|$ in Eq. (7) is a simple choice for an even function that is zero at $k=0$, has a peak at $k=k_0$, and is negative for large k. The presence of the factor $\phi(k)$ allows $\overline{f}$ to change sign with k, and its form in Eq. (8) is a simple (rather arbitrary) choice for a function that is even in k and changes sign as we change k. The factor ϕ introduces a second length scale in our model, and leads to patterns besides stripes [31]. The model has two dimensionless parameters r and k_c/k_0, whose variations, we find numerically (Sec. V), play roles analogous to varying the dimensionless acceleration Γ and the frequency f_0 of the drive in the experiment.

Our observation (Sec. V), that variation of r in our model plays a role similar to variation of Γ in the experiment, is suggested by our previous discussion of the single inelastic ball problem. Our observation that the variation of k_c/k_0 in the model plays a role similar to a variation of the drive frequency in the experiment is suggested if we suppose that the ratio k_c/k_0 arises from the ratio $a/l=f_0^2a/g$, of the two natural lengths in the system. The important observation is that this implies that k_c/k_0 varies monotonically with f_0 and is independent of the drive amplitude.

As will become clear from the theory (Secs. VI–IX), the important bifurcation phenomena are independent of the specific choices in Eqs. (5)–(8). We emphasize that we view Eqs. (1)–(8) as a minimalist model, and that several obvious generalizations immediately suggest themselves [e.g. a two-or higher-dimensional map replacing the one-dimensional map Eq. (1)]. Our point is that even this simple representation is rich enough to display many of the experimentally observed effects, and that certain of these effects can be regarded as physics independent and universal for systems in which patterning and period doubling interact. We will return to the discussion of this point in Sec. X.

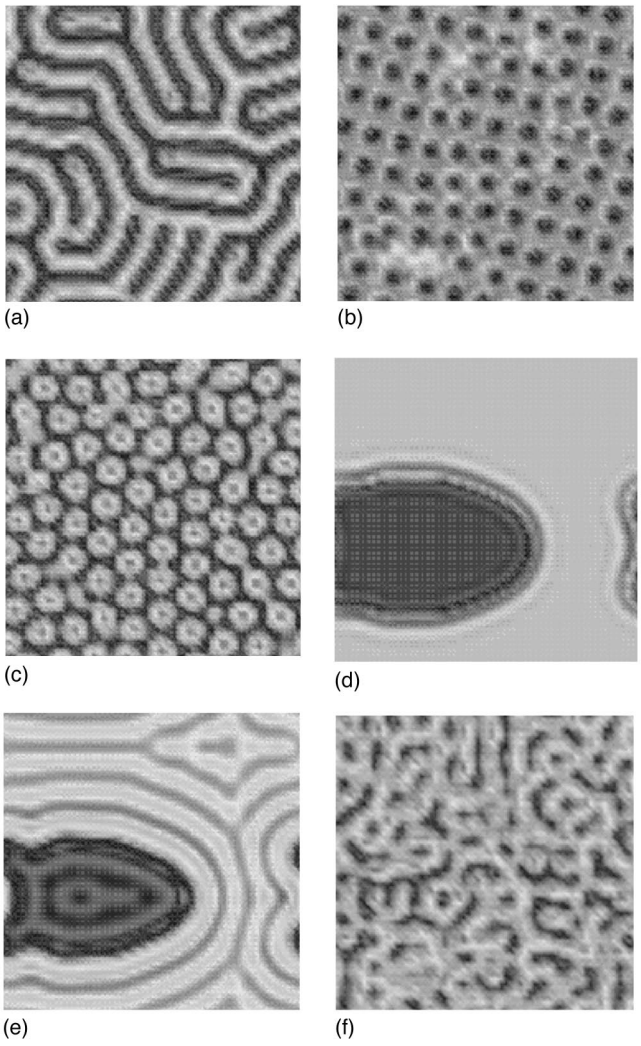

FIG. 3. Extended patterns obtained numerically in our model. (a) Period-2 stripes at $r=1.9$, $(k_c/k_0)^2=5$. (b) Period-2 squares at $r=1.9$, $(k_c/k_0)^2=1.5$. (c) Period-2 hexagons at $r=2.05$, $(k_c/k_0)^2=2.6$. (d) Period-2 flat state with a kink at $r=2.4$, $(k_c/k_0)^2=5$ (the kink is the border region between the high ξ and the low ξ areas). (e) Period-4 stripes at $r=2.7$, $(k_c/k_0)^2=5.0$. (f) Disorder at $r=3.2$, $(k_c/k_0)^2=5$.

V. NUMERICAL SIMULATION

Figures 3(a)–3(f) show numerical results from our model as r and k_c/k_0 are changed. These pictures are qualitatively similar to those in Ref. [10]. We regard as particularly significant the fact that, in our model, as we increase r, the bifurcation sequence is a period-1 flat state bifurcating to give a period-2 pattern which then becomes a period-2 flat state and eventually a period-4 pattern. Thus, *with an increase of the parameter, the period-2 and -4 patterns are separated by a period-2 flat state*. This basic sequence, also observed in the experiment, is universal in that it does not depend on the details of the model. In particular, it is present even with $\phi(k)$ removed, i.e., $\overline{f}(k)=\exp[\gamma(k)]$.

Figure 4 shows the approximate locations in the two parameter space $[r,(k_c/k_0)]$ of the various spatiotemporal behaviors numerically exhibited by our model. We note that, if

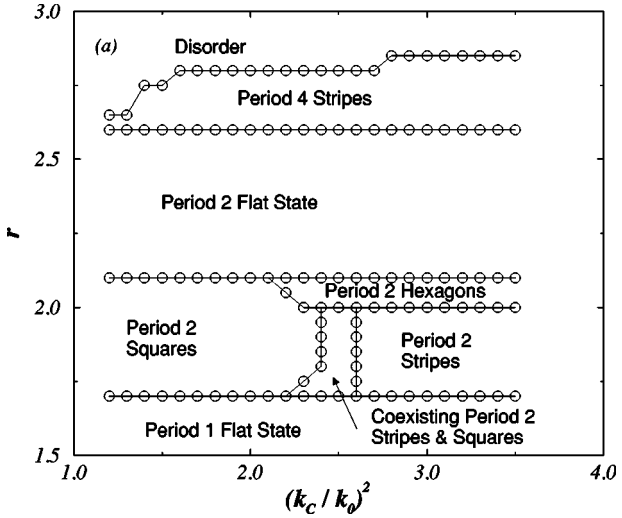

FIG. 4. Phase diagram showing the various stable patterns seen in numerical simulations with the model [Eqs. (1)–(8)].

we crudely identify r with the experimental dimensionless acceleration Γ and k_c/k_0 with the experimental frequency f_0, then there is striking qualitative agreement between the phase diagram obtained numerically from our model (Fig. 4) and the experimental phase diagram for thin layers (Fig. 1). In what follows, we consider a range $k_c/k_0>1$, corresponding to $\overline{f}(k_0)>1$.

The phases in Fig. 4 correspond to states that evolve from starting at a small initial perturbation about a homogeneous state. If, on the other hand, we follow large amplitude states with slow parameter changes, then we find that some of the transitions that are nonhysteretic in the experiment show substantial hysteresis in the model. We will discuss this aspect further in Sec. X, when we consider extensions of this simple model.

Other behaviors are observed experimentally when thicker layers are vibrated [11,12]. In particular, the experiments observe *oscillons*—localized period-2 structures on a period-1 flat background state, in the transition between the period 1-flat state and the period-2 patterns. For thick layers, this transition is significantly hysteretic and the oscillons exist in the transition region.

The bifurcations for the map in Eq. (5) (i.e., the bifurcations of the full system at $k=0$) are all supercritical. As we shall see in Sec IX, this implies that there is no hysteresis in the transition between the period-1 flat state and the period-2 patterns. We can incorporate hysteresis into our model by changing the map M to one which has a subcritical (hysteretic) period doubling from the fixed point. As an example, the map

$$M(\xi,r)=-(r\xi+\xi^3)\exp(-\xi^2/2) \tag{9}$$

has a subcritical period doubling from the fixed point. Figure 5 is a schematic representation of the bifurcation diagram for this map. With this map used in place of Eq. (5), we see period-2 localized states in the regime where the period-1 homogeneous state and the period-2 square state are both

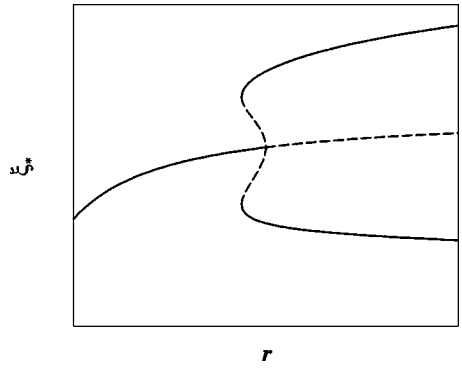

FIG. 5. The bifurcation diagram for a map with a hysteretic period doubling.

stable to small perturbations. These structures are similar to the oscillons seen in the experiments.

Figure 6(a) shows two oscillons in opposite temporal phases, and Fig. 6(b) shows a bound state of several close oscillons. We note that Tsimring and Aronson [23] and Crawford and Riecke [28] also obtained oscillons with a subcritical period doubling. It thus appears that subcriticality may be key to the oscillon phenomenon. As noted above, the oscillons that we find numerically in our model are stable in the parameter range of the hysteretic transition from the period-1 flat state to the period-2 patterns, as in the experiments.

VI. SUMMARY OF THE RESULTS

In the remainder of this paper, we will analyze various aspects of the pattern formation that we observe in our model. In Sec. VII, we perform a linear stability analysis about the spatially homogeneous periodic solutions of the system. From this analysis, we deduce the onset criteria for the period-2 and -4 patterns that are observed in our simulations. We also show that, generically, the bifurcation scenario on increasing the driving is period-1 homogeneous state→period-2 patterned state→period-2 homogeneous state→period-4 patterned state, explaining this characteristic feature of the experimental phase diagram. In Sec. VIII, we deduce a framework for a weakly nonlinear analysis of our model. Using group-theoretic considerations of the underlying symmetries of the system, we show that a truncated

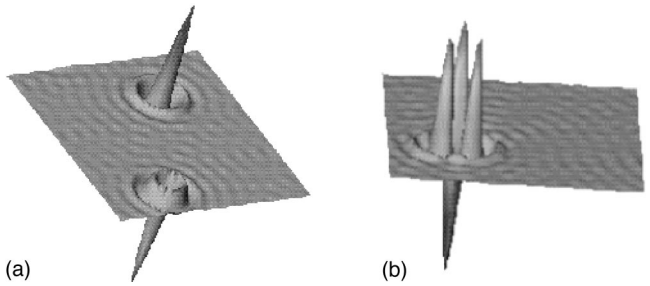

FIG. 6. Localized states obtained using a map with subcritical bifurcations. (a) Two oscillons out of phase [$r=0.65$, $(k_c/k_0)^2=1.7$]. (b) A bound state with coordination number 3 [$r=0.55$, $(k_c/k_0)^2=1.7$].

modal expansion can be used to study the selection of various patterns in different parameter regimes.

In Sec. IX, we specialize to the case of period-2 patterns. Close to the onset of the patterns, there is a strong separation of the time scales for the evolution of the amplitudes of the various modes in the truncated modal expansion. We show that the evolution of the pattern on a long time scale is determined by the dynamics of a small number $[O(1)]$ of dominant modes, and that the amplitudes of the rest of the modes are slaved to the the amplitudes of the dominant modes. This technique greatly simplifies the determination of the selected patterns. It also enables us to study the bifurcations between the various patterned regimes.

We will now list some of the principal results form our analysis. These results are scaling laws for various quantities that are valid close to bifurcations. The scaling laws are in terms of a supercriticality parameter ϵ. ϵ is defined so that the linear growth of the amplitude $a_n(\mathbf{k})$ of the fastest growing modes is given by $|a_{n+1}(\mathbf{k})|/|a_n(\mathbf{k})|=(1+\epsilon)$. The onset of the pattern is thus given by $\epsilon=0$.

(1) The case of one dominant mode corresponds to stripe solutions. We present explicit solutions to the weakly nonlinear equations. These equations give the scaling

$$h_{\mathrm{st}}\sim\epsilon^{1/2}$$

for the stripe amplitude h_{st} close to onset. We also discuss the symmetry properties of the stripe patterns.

(2) The case of two dominant modes corresponds to rhombus and square patterns. We show that square patterns form generically, i.e., without any fine tuning of parameters. We present explicit solutions for these patterns that give the scaling law

$$h_{\mathrm{rh}}\sim\epsilon^{1/2}$$

for the pattern amplitude h_{rh} near onset. We discuss the bifurcation between the stripe and the square solutions, and show that it is nonhysteretic as a bifurcation between steady states, that is, in the limit that the run time $T\to\infty$. We also deduce the scaling law

$$\Delta p\sim(\epsilon T)^{-1},$$

where Δp is the apparent hysteresis in a generic parameter at the transition between the stripe and rhombus (square) solutions for experiments run for a finite duration T. We also show the existence of *transient stripes*, that is patterns that are asymptotically square patterns, but look like stripes in a transient stage of their evolution.

(3) The case of three dominant modes with an additional imposed symmetry corresponds to hexagonal patterns. We show that there is a hexagonal pattern solution near the onset of period-2 patterns, but it is linearly unstable to the stripe patterns, thereby explaining why we do not see hexagonal patterns near the onset of the period-2 patterns.

(4) We also analyze a model that corresponds to the two frequency forcing experiments [10]. We show that breaking the discrete time translation symmetry $t\to t+1/f_0$ where f_0 is the frequency of the dominant forcing can lead to the formation of stable hexagonal patterns, as seen in the experiments. The crossover between the behavior corresponding to no symmetry breaking and stripe patterns, to the behavior with symmetry breaking and stable hexagons is given by

$$\Delta\sim\epsilon^{1/2},$$

where Δ is a measure of the symmetry breaking (say the ratio of the amplitudes of the f_0 and $f_0/2$ components of the drive.)

We believe that these scaling laws, especially the crossover behavior for the two frequency forcing, can be verified experimentally. In the experiments, the parameter ϵ is given by

$$\epsilon\sim|\Gamma-\Gamma_c|,$$

where Γ_c is the value of the parameter Γ at the relevant bifurcation.

In our analysis, we also discuss various symmetry considerations for the various patterns. Experimentally observable consequences of these symmetries include the occurrence or nonoccurrence of fronts separating domains of patterns with different temporal phases [10].

VII. STABILITY ANALYSIS FOR THE ONSET OF PATTERNS

We will first investigate the stability of the spatially homogeneous and temporally periodic states to the formation of spatially patterned states. This analysis will give criteria for the onset of patterned states. It will also explain the separation of the patterned period-2 and patterned period-4 states by a period-2 homogeneous state.

For a given value of r, let the one-dimensional map $M(\xi,r)$ have a stable period-p periodic orbit $\xi_1,\xi_2,\ldots,\xi_p$. Then $M(\xi_p,r)=\xi_{p+1}=\xi_1$. The stability index of the periodic orbit is given by

$$\lambda_p(r)=N(\xi_1)N(\xi_2)\cdots N(\xi_p),$$

with

$$N(\xi)=\frac{\partial M(\xi,r)}{\partial\xi}.$$

Since the orbit is assumed to be stable, it follows that $|\lambda_p(r)|<1$. Recall that at a period doubling of a period-p orbit to a period-$2p$ orbit, the stability index of $\lambda_p(r)$ decreases through -1. Furthermore, for the map in Eq. (5) and $p=1,2,3,\lambda_p(r)$ decreases monotonically with r.

For our spatiotemporal model [Eqs. (1)–(8)], we now consider the stability of the sequence of spatially homogeneous states $\xi_i(\mathbf{x})=\xi_i$ to small perturbations, so that $\xi_n(\mathbf{x})=\xi_n+\delta\xi_n(\mathbf{x})$. Equation (1) yields

$$\delta\xi'_{n+1}(\mathbf{x})=N(\xi_n)\,\delta\xi_n(\mathbf{x}).$$

Equation (2) yields

$$\delta\overline{\xi}_{n+1}(\mathbf{k})=N(\xi_n)\overline{f}(\mathbf{k})\,\delta\overline{\xi}_{\mathbf{n}}(\mathbf{k}).$$

After p iterations, we have

$$\delta\overline{\xi}_{n+p}(\mathbf{k}) = \lambda_p(r)[\overline{f}(k)]^p \delta\overline{\xi}_n(\mathbf{k}).$$

Since $|\overline{f}(k)|$ has a peak at $k=k_0$, it follows that the period-p spatially homogeneous states are stable to spatially varying perturbations if $|\lambda_p(r)[\overline{f}(k_0)]^p|<1$. It also follows that the wave vectors $\mathbf{k}$ with the largest growth rate have $|\mathbf{k}|=k_0$. Consequently, the spatially homogeneous state will become unstable to a spatially varying (patterned) state for $|\lambda_p(r)[\overline{f}(k_0)]^p|>1$.

When the spatially homogeneous state becomes unstable, close to onset, the patterned state will consist of wave vectors $\mathbf{k}$ with $|\mathbf{k}|$ close to k_0. The period-p spatially homogeneous states are unstable to a period p spatially varying state if $\lambda_p(r)[\overline{f}(k_0)]^p>1$, and are unstable to a period-$2p$ pattern if $\lambda_p(r)[\overline{f}(k_0)]^p<-1$.

We will now consider the bifurcation scenario as r is varied through the range over which the period-p orbit is stable for the map M. We will assume that the period-p orbit is created by a period doubling from a period-$p/2$ orbit, and that it becomes unstable by period doubling to a period-$2p$ orbit. The period-p orbit is born (first becomes stable) at a value of $r=r_-$ such that $\lambda_p(r_-)=1$. It becomes unstable to a period-$2p$ orbit by period doubling at $r=r_+$ such that $\lambda_p(r_+)=-1$. At this point, $\lambda_{2p}(r_+)=(\lambda_p(r_+))^2=1$, so that a period-$2p$ orbit is born. If the map M is smooth, $\lambda_p(r)$ will vary smoothly as a function of r in the range $[r_-,r_+]$. Consequently, there is a value r_0 in this range such that $\lambda_p(r_0)=0$. At this value of r, the period-p orbit is said to be superstable.

At the superstable point,

$$\lambda_p(r_0)[\overline{f}(k_0)]^p=0.$$

Consequently, there is a range of r values around r_0 such that $|\lambda_p(r)[\overline{f}(k_0)]^p|<1$, and, in this range, the homogeneous period-p state is stable to all small perturbations.

Since $\overline{f}(k_0)>1$, it follows that

$$\lambda_p(r_-)[\overline{f}(k_0)]^p>1.$$

Consequently, there is a range of r values including r_- but less than r_0, such that $\lambda_p(r)[\overline{f}(k_0)]^p>1$; in this range, the homogeneous period-p state is unstable to a period-p patterned state. Also,

$$\lambda_p(r_+)[\overline{f}(k_0)]^p<-1,$$

so that there is a range of r values including r_+ but greater than r_0, such that $\lambda_p(r)[\overline{f}(k_0)]^p<-1$, and in this range, the homogeneous period-p state is unstable to a period-$2p$ patterned state.

We will illustrate the above bifurcation scenario for period-1 and -2 homogeneous states. Figure 7(a) is a bifurcation diagram for a generic map $M(\xi,r)$ that undergoes a supercritical period doubling [e.g., Eq. (5)], and Fig. 7(b) schematically shows the stability index for attracting periodic orbits (or fixed points) versus r. At $r=r_a$, the period-1 orbit of the map is superstable so that $\lambda_1(r_a)=0$. As we increase r, at $r=r_c$, $\lambda_1(r_c)=-1$, and the map M undergoes a period doubling. On further increasing r, the period-2 orbit becomes superstable at $r=r_e$, so that $\lambda_2(r_e)=0$.

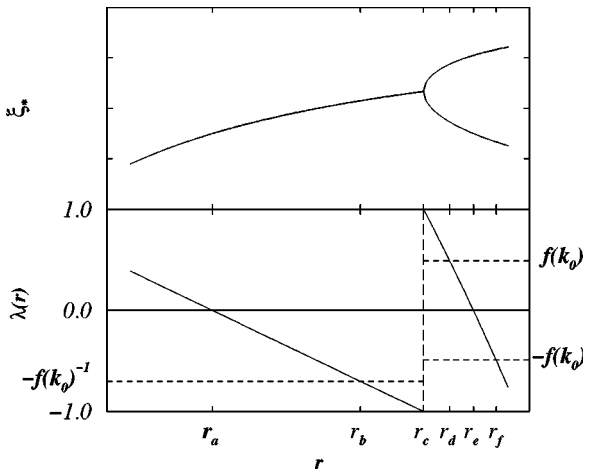

FIG. 7. (a) Schematic bifurcation diagram near a period doubling. (b) The stability index $\lambda(r)$ for the stable periodic (fixed) points.

r_b satisfies $r_a<r_b<r_c$, and is such that $\lambda_1(r_b)\overline{f}(k_0)=-1$. Therefore, the period-1 homogeneous state becomes unstable to a period-2 pattern at $r=r_b$. r_d is in the range $r_c<r_d<r_e$, and it satisfies $\lambda_2(r_d)\overline{f^2}(k_0)=1$. At this point, the period-2 homogeneous state becomes stable. On further increasing r, there exists a parameter value r_f with $r_f>r_e$, such that $\lambda_2(r_f)\overline{f^2}(k_0)=-1$. At this value of r, the period-2 homogeneous state becomes unstable to a period-4 pattern.

As is evident from this argument, for models in this framework, we should generically expect the following bifurcation scenario: period-1 homogeneous state→period-2 patterned state→period-2 homogeneous state→period-4 patternedstate. Note that this conclusion does not depend on the precise details of the model, namely, the functions f and M. Also note that, since these are generic bifurcations, this sequence is stable to system perturbations that destroy the special form of our CCM model; i.e., a local period doubling nonlinear map followed by a linear spatial coupling.

VIII. ANALYSIS OF EXTENDED PATTERNS

The elementary stability considerations in Sec. VII give us the basic bifurcation scenario and also the values of the parameter r at which there are bifurcations between flat states and patterned states. Although the stability analysis indicates that patterns with a length scale $1/k_0$ are formed, it does not give us any information on the nature of the patterns.

In this section we will analyze the model further and determine the patterns that are selected near onset. If we consider the model on a square region $(x,y)\in[0,L]\times[0,L]$ with periodic boundary conditions, the scalar field ξ can be expressed in terms of the Fourier modes as

$$\xi_n(\mathbf{x}) = \sum_{(i,j)\in\mathbb{Z}^2} \overline{\xi}_n(\mathbf{k}_{ij}) e^{i\mathbf{k}_{ij}\cdot\mathbf{x}}, \tag{10}$$

where $\mathbb{Z}^2$ is the integer lattice in two dimensions, and

$$\mathbf{k}_{ij} = \left(\frac{2\pi i}{L}, \frac{2\pi j}{L} \right).$$

Since ξ_n is real, it follows that $\overline{\xi}_n(-\mathbf{k}) = \overline{\xi}_n^*(\mathbf{k})$, where $\overline{\xi}^*$ is the complex conjugate of $\overline{\xi}$. We will assume that the square region is much larger than the wavelength of the pattern, that is $k_0 L \gg 1$.

In order to determine the selection of patterns, we need to look at the equations for the evolution of the amplitudes $\overline{\xi}_n(\mathbf{k})$ beyond the linear order. A formal procedure would be as follows.

(1) Drop the terms in the Fourier series with $|k_{ij}| \gg k_0$. [Since $\overline{f}(k) \ll 1$ for $k \gg k_0$, these modes are strongly damped in every iteration.] This converts the infinite sum to a finite sum with $O[(k_0 L)^2]$ terms.

(2) Expand the nonlinear equations that specify our model in powers of the mode amplitudes $\overline{\xi}_n(\mathbf{k})$, and retain the lowest order terms.

This, however, is not a practical framework for the analytical study of pattern selection, because we will obtain $O[(k_0 L)^2]$ nonlinear equations with the mode amplitudes $\overline{\xi}_n(\mathbf{k})$ as dynamical variables. We therefore need to significantly reduce the number of degrees of freedom that we have to consider. The procedure that we use to carry out this reduction is analogous to the procedure used in PDE models of pattern forming systems where the patterns are represented by amplitude equations which are then analyzed in the weakly nonlinear regime [1].

We motivate our reduction procedure by considering the results from a typical simulation of the model. Figure 8 shows the evolution of a pattern from an initial state that is spatially homogeneous with a small random perturbation. We use three quantities, δ_n, β_n, and K_n that are defined below, to characterize the evolution of the pattern. The typical amplitude of the pattern $\xi_n(\mathbf{x})$ is given by the mean square fluctuation

$$\delta_n^2 = L^{-2} \int \xi_n^2(\mathbf{x}) d\mathbf{x} - L^{-2} \left(\int \xi_n(\mathbf{x}) d\mathbf{x} \right)^2$$

$$= \sum_{(i,j)\in\mathbb{Z}^2} |\overline{\xi}_n(\mathbf{k}_{ij})|^2 - |\overline{\xi}_n(\mathbf{0})|^2.$$

We measure the deviation from temporal periodicity by the (normalized) quantity

$$\beta_n^2 = \frac{1}{\delta_n^2 L^2} \int [\xi_{n+p}(\mathbf{x}) - \xi_n(\mathbf{x})]^2 d\mathbf{x},$$

where p is the presumed periodicity of the system. Finally, we define the effective number of modes to be

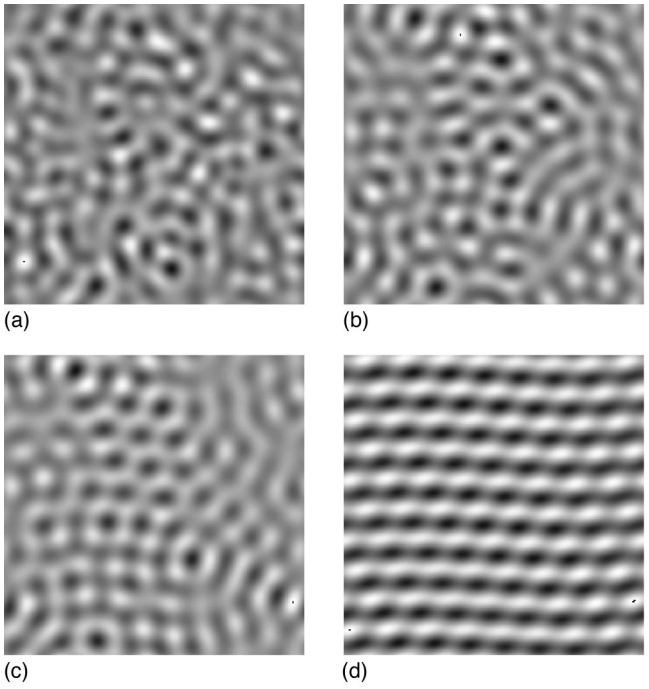

FIG. 8. Various regimes in the formation of a pattern, starting from a random, close to homogeneous, initial condition. The parameters are $r = 1.73$, $(k_c/k_0)^2 = 2.5$. (a) The pattern after ten iterations. (b) The patterns after 10^2 iterations. (c) The patterns after 10^3 iterations. (d) The patterns after 10^4 iterations.

$$K_n = \frac{1}{2} \left(\frac{\delta_n^2}{\max_{(i,j)\in\mathbb{Z}^2,(i,j)\neq(0,0)} |\overline{\xi}_n(\mathbf{k}_{ij})|^2} \right).$$

The factor 1/2 in the definition of K_n is to account for the fact that ξ_n is real, and this implies $\overline{\xi}_n(-\mathbf{k}) = \overline{\xi}_n(\mathbf{k})$, which is effectively one (complex) mode amplitude.

Figures 9, 10, and 11 show the evolution of the quantities

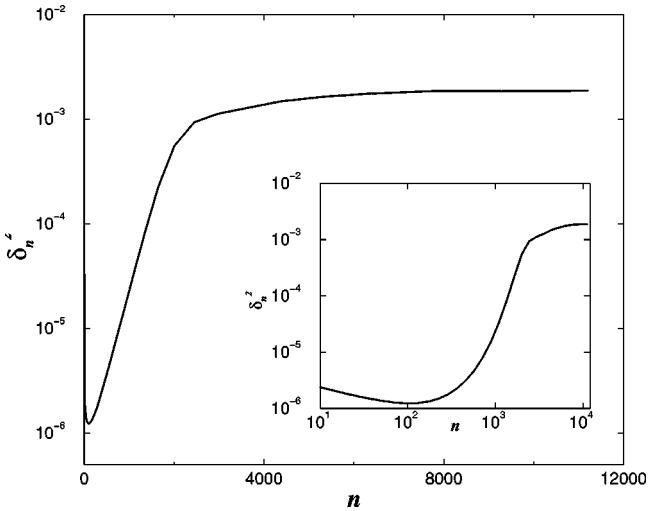

FIG. 9. The evolution of δ_n^2 with the time index n for the simulation depicted in Fig. 8.

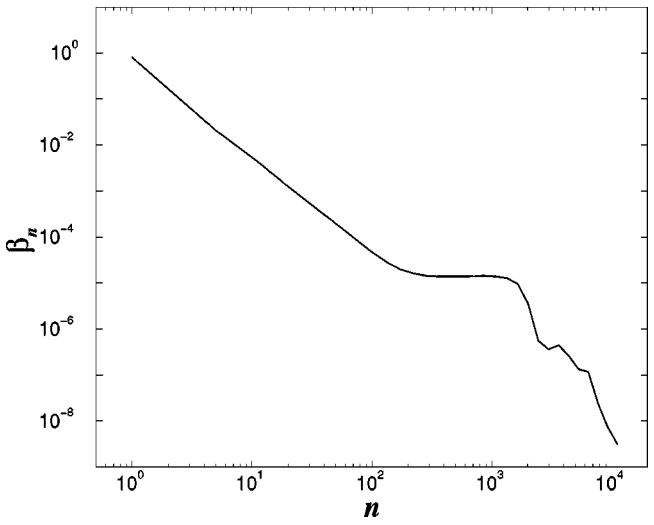

FIG. 10. The deviation from periodicity vs n for the simulation depicted in Fig. 8.

δ_n, β_n, and K_n for the dynamics illustrated in Fig. 8. There appear to be four regimes in the evolution of a patterned state.

(1) There is a short initial transient for $n \lesssim 100$. At this stage, the mode amplitudes of the wave vectors with $|\mathbf{k}|$ sufficiently different from k_0 decay rapidly, and the quantities δ_n^2, β_n^2, and K_n all decrease rapidly.

(2) Phase (1) is followed by a phase of exponential growth of δ_n^2 for $100 \lesssim n \lesssim 2000$. In this regime, the amplitudes of all the unstable modes grow in accordance with the predictions from the linearization about the homogeneous state that was considered in Sec. VII. The growth rate for the modes with $k=k_0$ in this phase is given by $\log(|\lambda(r)\overline{f}(k_0)|)$, so that the associated time scale is

$$\tau = \frac{1}{\log[|\lambda(r)\overline{f}(k_0)|]}.$$

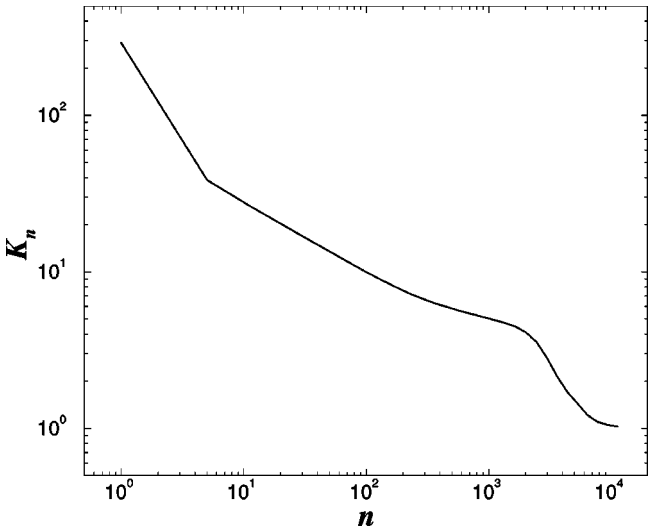

FIG. 11. The dependence of the effective number of modes on the time index n for the simulation depicted in Fig. 8.

For our choices of parameter, $\tau \approx 400$. In this regime, no pattern has yet been selected. β_n is approximately a constant in this regime.

(3) After about 2000 iterations, the growth of δ_n^2 saturates. To a good approximation, the system is in a periodic state. In this intermediate regime, the nonlinearities in the dynamics have selected a pattern, in this case a stripe pattern. However, this pattern is not ''global,'' in that the stripes do not have the same orientation through out the square. Rather, they have domains of constant orientation, and the typical length scale of a constant orientation domain is on the order of a few wavelengths.

(4) There is a slow coarsening process for $10^3 \lesssim n \lesssim 10^4$, wherein the domains compete, with some of them growing at the expense of the others. After about 10^4 iterations, which is on a time scale $T \gg \tau$, one domain takes over the entire square region. The system is now in a periodic steady state, and in this regime the stripes are globally lined up.

A. Local degrees of freedom

The preceding discussion shows that the dynamics of the system has multiple spatial and temporal scales. Further, in order to describe the pattern selection in this system, we need to look at the dynamics in the intermediate regime where the amplitude of the patterns have saturated, but the patterns are not yet ''global.''

For a stripe pattern, we would expect three degrees of freedom—the stripe amplitude, phase, and orientation—to be sufficient in order to describe the pattern. For the intermediate regime $n \approx 10^3$, we see that $K_n > 1$ for the simulation illustrated in Figs. 8 and 11. This is due to the fact that there are many domains each of which has a stripe pattern, but with an independent orientation and amplitude. This makes it hard to describe the dynamics of this regime, since we need to describe the dynamics of many degrees of freedom. In contrast, for $n \approx 10^4$, $K_n \approx 1$ to within a few percent. Therefore, we expect that it is much simpler to describe this regime. The large number of effective degrees of freedom in the intermediate quasi-steady state is due to the following two features in our model.

(1) The dynamics given by the map M in Eq. (1) is purely local, and the function $f(\mathbf{x})$ in Eq. (3) is short ranged with an effective interaction range $\approx k_0^{-1}$. Consequently, if we divide the square region into domains that have a length scale l satisfying $k_0^{-1} \ll l \ll L$, the dynamics on each of these smaller domains is largely independent of the dynamics on the other domains, at least for the time scales corresponding to the initial growth of the modes, which is the time scale at which patterns first appear.

(2) If $k_0 L \gg 1$, the boundaries do not play a significant role in the dynamics. In this case, the model is exactly invariant under time translations by one time step, and is approximately invariant under spatial translations, rotations, and reflections about arbitrary directions.

As a consequence of remark (2) above, the symmetry group for the equations on an infinite spatial domain, i.e., in the limit $L \to \infty$ is

$$\mathcal{G}=\mathbb{Z}\times\mathbb{R}^2\times O(2),$$

where the first factor $\mathbb{Z}$ is from the (discrete) time translation symmetry, the second factor is the translation group in two dimensions, and the third factor is the approximate symmetry under rotations and reflections. If $g\in\mathcal{G}$ is an element of the symmetry group, then $g=(m,\mathbf{a},M)$, where m is an integer, $\mathbf{a}\in\mathbb{R}^2$, and M is a 2×2 orthogonal matrix. The action of an element $g=(m,\mathbf{a},M)$ on the scalar field $\xi_n(\mathbf{x})$ is given by

$$S_g[\xi_n(\mathbf{x})]=\xi_{n'}(\mathbf{x}')$$

where $n'=n+m$ and $\mathbf{x}'=M\cdot(\mathbf{x}+\mathbf{a})$. We will henceforth refer to $\mathcal{G}$ as the symmetry group of the dynamical system, on a finite domain of size L, even though this is strictly true only in the limit $L\to\infty$.

A consequence of this (approximate) symmetry is that, even if we are in a parameter regime with a unique stable pattern P that is an attractor for the system, there is degeneracy in the asymptotic states of the system associated with the symmetries of the equations.

The degeneracies due to the symmetries of the system, along with the short range of the interaction imply that it is possible to sustain different solutions in different spatial domains for time intervals that are long compared to the time scale for the initial growth. In a parameter regime where a period-p pattern $P(\mathbf{x},n \bmod p)$ is the unique stable pattern, the intermediate quasi-steady-state is described by the following ''domain decomposition.''

(1) The square $R=[0,L]^2$ is divided into domains D_i, $i=1,2,\ldots,M$.

(2) On each domain D_i, away from the boundaries of the domain, the scalar field $\xi_n(\mathbf{x})$ is close to the scalar field $\xi^i_\infty(\mathbf{x},n \bmod p)$ of a ''global'' pattern, that is a pattern which is a stable, asymptotic, period p steady state.

(3) The domains D_i as well as the asymptotic pattern ξ^i_∞ on the domain D_i are nearly unchanged over the time scale τ, the characteristic time for linear growth of the modes. Here the patterns ξ^i_∞ are given by the action of a symmetry transformation on the pattern P. This notion can be formalized as follows. Let $\mathcal{S}$ denote the set of all the solutions $\xi_\infty(\mathbf{x},n)$ that are equivalent to $P(\mathbf{x},n)$ modulo the action of a symmetry transformation in $\mathcal{G}$. Let $G\subseteq\mathcal{G}$ denote the *isotropy subgroup* for the pattern P, that is the set of all the elements of $\mathcal{G}$, that leave P invariant [32]. Then G is the symmetry group of the pattern P, since

$$S_g[P(\mathbf{x},n)]=P(\mathbf{x},n)$$

for all $g\in G$. G is a normal subgroup of $\mathcal{G}$ [32]. The quotient group $\mathcal{P}=\mathcal{G}/G$, is the set of all the transformations between the elements of $\mathcal{S}$, the set of distinct pattern solutions equivalent to $P(\mathbf{x},n)$ [32]. We will call $\mathcal{P}$ the transformation group of the solution set $\mathcal{S}$, and every element $g\in\mathcal{P}$ gives a solution $\xi_n(\mathbf{x})$ equivalent to P by

$$\xi_n(\mathbf{x})=S_g[P(\mathbf{x},n)].$$

From our earlier discussion, the pattern on each domain D_i is characterized by an element $g_i\in\mathcal{P}$. We can define a field of the symmetry elements

$$g(\mathbf{x},n)=\sum_i g_i(n)\chi_{D_i(n)}(\mathbf{x}), \tag{11}$$

where $\chi_A(\mathbf{x})$ is the indicator function for the set A. From our discussion above, it follows that $g(\mathbf{x},n)$ does not vary significantly over a length scale $l\gg k_0$ and a time scale $T\gg\tau$. Therefore, we can coarse grain the field g over these scales to obtain a smooth, slowly varying function $\tilde{g}(\mathbf{x},n)$. To describe the quasisteady intermediate state and the approach to the asymptotic periodic pattern, it suffices to consider the dynamics of $\tilde{g}(\mathbf{x},n)$. We will call the field $\tilde{g}$ the *local degrees of freedom* of the system. We will make these arguments mathematically rigorous by doing a multiple time scale analysis of the system in a future publication, where we will also determine the dynamical equation for the field $\tilde{g}$ [33].

The domain decomposition effectively decouples the dynamics of the pattern in the intermediate state from the pattern selection problem. The pattern selection problem reduces to finding the appropriate asymptotic pattern P, and a description of the dynamics in the intermediate state is given by the dynamics of the field $\tilde{g}$ which does not play a role in determining the pattern P. In what follows our concern is with determining the stable pattern P.

B. Truncated modal expansions

We have argued that, in order to determine the selection of patterns, it suffices to find the stable global pattern P. Since the patterns are selected in the initial phase on a time scale τ and the dynamics are such that there is no significant interaction between domains of size $l\gg k_0^{-1}$ on a time scale τ, it suffices to restrict our attention to such a domain and look at the pattern that is selected on this domain. Note that a domain of size $l\gg k_0^{-1}$ is sufficiently large in order to discern patterns with a scale k_0^{-1}. We now attempt to determine the pattern selected on such a domain as well as determine the dynamics in the initial transient growth stage leading to the formation of the selected pattern.

Given a domain D with a length scale l, we see that $e^{i\mathbf{k}_1\cdot\mathbf{x}}\approx e^{i\mathbf{k}_2\cdot\mathbf{x}}$ for all $\mathbf{x}\in D$ if $|\mathbf{k}_1-\mathbf{k}_2|\ll1/l$. Therefore, we can coarse grain the Fourier mode amplitudes over a region of size smaller than $1/l$ in Fourier space. Let $\mathbf{k}$ be in the center of $\mathcal{K}$, a coarse-grained region in Fourier space. If the point $\mathbf{x}_0$ in the domain D is such that D is contained in a disk centered at $\mathbf{x}_0$ of radius l, we define $b_n(\mathbf{k})$, the coarse-grained amplitude for the region $\mathcal{K}$, by requiring that

$$b_n(\mathbf{k})e^{i\mathbf{k}\cdot\mathbf{x}_0}\approx\sum_{k_{ij}\in\mathcal{K}}\overline{\xi}_n(\mathbf{k}_{ij})e^{i\mathbf{k}_{ij}\cdot\mathbf{x}}$$

for all $\mathbf{x}\in D$. Setting $\mathbf{x}=\mathbf{x}_0$, we thus take $b_n(\mathbf{k})$ to be

$$b_n(\mathbf{k})=\sum_{\mathbf{k}_{ij}\in\mathcal{K}}\overline{\xi}_n(\mathbf{k}_{ij})e^{i(\mathbf{k}_{ij}-\mathbf{k})\cdot\mathbf{x}_0}. \tag{12}$$

From the symmetries of $\overline{\xi_n}$, we have $b_n(-\mathbf{k})=b_n^*(\mathbf{k})$. From Eqs. (12) and (10), we see that on the domain D, the scalar field ξ is given by

$$\xi_n(\mathbf{x}) \approx \sum_{\mathbf{k}_m \in C} b_n(\mathbf{k}_m) e^{i\mathbf{k}_m \cdot \mathbf{x}}, \tag{13}$$

where the set C is the set of the centers of the coarse-grained regions in Fourier space that contribute significantly to the sum in Eq. (10). Equation (13) is a *truncated modal expansion* for ξ on a domain D. In general, the size of C is small and the number of terms in this sum for a pattern P is of the same order as the number K_n in the periodic regime at long times. Therefore, this is an effective way to reduce the number of degrees of freedom. However, this expansion gives a description that is valid even in the initial stages of the pattern selection. Note that, unlike the amplitudes of the Fourier modes which are defined on an integer lattice, the set C is not *a priori* restricted to be of any particular geometric form.

IX. PERIOD-2 PATTERNS

Our discussion of pattern selection up to this point has been general and is valid for all parameter regimes of our model. We will now restrict ourselves to the pattern selection problem for period-2 patterns.

We begin by considering the parameter regime near onset of the period-2 patterns. From our discussion in Sec. VII, we see that the parameter $r=r_b$ at onset is given by $\lambda(r_b)\overline{f}(k_0)=-1$. For $r>r_b$, $\lambda(r)\overline{f}(k_0)<-1$. We define a supercriticality parameter ϵ by

$$\epsilon = -\lambda(r)\overline{f}(k_0) - 1.$$

We can define a mode-dependent growth rate by

$$\alpha(\mathbf{k},r) = \lambda(r)\overline{f}(|\mathbf{k}|).$$

Then $\alpha(\mathbf{k},r)=-(1+\epsilon)$ if $|\mathbf{k}|=k_0$. We will assume that we are sufficiently close to onset ($r-r_b$ is sufficiently small) so that for a $\eta \approx 1/l$ and a $\mu \gg 1/\tau$, we have

$$\alpha(\mathbf{k},r) > -1+\mu \quad \text{if} \quad \big||\mathbf{k}|-k_0\big| > \eta. \tag{14}$$

This is always possible since τ is very large near the onset, and $|\alpha(\mathbf{k},r)|$ has a single peak at $|\mathbf{k}|=k_0$. From this point, we will keep r fixed and suppress the dependence of the various quantities on r, i.e., for example, we denote $\lambda(r)$ by λ.

We can expand the nonlinear map in Eq. (1) about the (stable) fixed point ξ_* to obtain

$$M(\xi,r) - \xi_* = \lambda(\xi-\xi_*) + \beta(\xi-\xi_*)^2 + \gamma(\xi-\xi_*)^3 + O[(\xi-\xi_*)^4]. \tag{15}$$

For reasons that will become clear below, we need to expand to third order in $\xi-\xi_*$.

From the modal expansion in Eq. (13), we see that

$$\xi_n(\mathbf{x}) - \xi_* = b_n(\mathbf{0}) - \xi_* + \sum_{\mathbf{k}_m \in C, \mathbf{k} \neq \mathbf{0}} b_n(\mathbf{k}_m) e^{i\mathbf{k}_m \cdot \mathbf{x}} = \sum_{\mathbf{k}_m \in C} a_n(\mathbf{k}_m) e^{i\mathbf{k}_m \cdot \mathbf{x}},$$

where $a(\mathbf{0})=b(\mathbf{0})-\xi_*$ and $a(\mathbf{k})=b(\mathbf{k})$ for $\mathbf{k} \in C, \mathbf{k} \neq \mathbf{0}$. Using this expression and Eq. (15) gives an expression for $\xi'_{n+1}(\mathbf{x})$ with errors of order a^4, where $a=\max_{\mathbf{k}\in C}|a_n(\mathbf{k})|$. We need to coarse grain this expression by the same regions that we used for defining $\xi_n(\mathbf{x})$ in order to keep a consistent modal expansion. This procedure is effected by setting $\mathbf{k} \approx \mathbf{k}_p$ where $\mathbf{k}$ is arbitrary and $\mathbf{k}_p \in C$, if $|\mathbf{k}-\mathbf{k}_p| < 1/l$. The linear operator $\mathcal{L}$ is given by

$$\mathcal{L}[e^{i\mathbf{k}_m \cdot \mathbf{x}}] = \overline{f}(|\mathbf{k}_m|) e^{i\mathbf{k}_m \cdot \mathbf{x}}.$$

for all $\mathbf{k}_m \in C$. Since $\mathcal{F}[\xi_n]=\mathcal{L}[M(\xi_n)]=\xi_{n+1}$, we can compare the terms of the modal expansions of $\mathcal{L}[M(\xi_n)]$ and ξ_{n+1} to obtain

$$\begin{aligned} a_{n+1}(\mathbf{k}) = {} & \alpha(\mathbf{k}) a_n(\mathbf{k}) \\ & + \overline{f}(|\mathbf{k}|) \Bigg(\beta \sum_{\mathbf{k}_1} \sum_{\mathbf{k}_2} I_b(\mathbf{k}_1+\mathbf{k}_2-\mathbf{k}) a_n(\mathbf{k}_1) a_n(\mathbf{k}_2) \\ & + \gamma \sum_{\mathbf{k}_1} \sum_{\mathbf{k}_2} \sum_{\mathbf{k}_3} I_b(\mathbf{k}_1+\mathbf{k}_2+\mathbf{k}_3-\mathbf{k}) \\ & \times a_n(\mathbf{k}_1) a_n(\mathbf{k}_2) a_n(\mathbf{k}_3) \Bigg) + O(a^4), \end{aligned} \tag{16}$$

where all the summations are over the relevant $\mathbf{k}_i$ in C, and I_b is an indicator function given by $I_b(\mathbf{k})=1$ if $|\mathbf{k}|<1/l$, and zero otherwise.

We will consider this equation for the modes with $\big||\mathbf{k}|-k_0\big| > 1/l$ and $|\mathbf{k}|=k_0$ separately. The linear analysis in Sec. VII suggests that the modes with the largest amplitudes have $|\mathbf{k}|=k_0$. In the initial stages of the growth, the evolution of a mode amplitude $a_n(\mathbf{k}_1)$ with $|\mathbf{k}_1|=k_0$ is given by

$$a_{n+1}(\mathbf{k}_1) = -(1+\epsilon) a_n(\mathbf{k}_1) + N[\{a_n(\mathbf{k})\}]. \tag{17}$$

where $N[\{a_n(\mathbf{k})\}]$ is a nonlinear term that depends on the set of mode amplitudes $\{a_n(\mathbf{k})\}$. This leads us to consider the inhomogeneous difference equation

$$a_{n+1} = \alpha a_n + f_n. \tag{18}$$

We can solve this equation to obtain

$$a_{n+1} = \alpha^{n+1} a_0 + \sum_{m=0}^{n} \alpha^{n-m} f_m. \tag{19}$$

Therefore, we can solve Eq. (17) to obtain

$$a_n(\mathbf{k}_1) = (-1)^n (1+\epsilon)^n a_0(\mathbf{k}_1) + \sum_{m=0}^{n-1} (-1)^{n-m-1} (1+\epsilon)^{n-m-1} N_m,$$

where N_m is the nonlinear term with the dependencies suppressed. The linearized solution obtained by neglecting the nonlinear terms is valid for n such that $n\epsilon \ll 1$ and $|N_n| \ll \epsilon |a_n(\mathbf{k}_1)|$. If the dominant nonlinearity is of the form $N(\{a_n\}) \sim a^p$, we see that the nonlinearities become important when $\epsilon a \sim a^p$, that is

$$a \sim \epsilon^{1/(p-1)}.$$

Therefore, to time scales of order $\tau \approx 1/\epsilon$ and amplitudes smaller that $\epsilon^{1/(p-1)}$, the mode amplitudes with $|\mathbf{k}| = k_0$ evolve independently of each other, and grow exponentially.

Once the nonlinearity N_n becomes comparable to $\epsilon a_n(\mathbf{k}_1)$, the evolution depends on the sign of the nonlinearity. From Eq. (17), we have

$$a_{n+2}(\mathbf{k}_1) - a_n(\mathbf{k}_1) = (2\epsilon + \epsilon^2) a_n(\mathbf{k}_1) + N_{n+1} - (1+\epsilon) N_n .$$

If the nonlinearity is confining, that is if the sign of $N_{n+1} - (1+\epsilon)N_n$ is the negative of the sign of a_n, the nonlinearity saturates the growth of the modes. Further, if the fixed point $a_{n+2} = a_n$ of the above equation is stable, we have a stable period-2 solution and the time scale on which the amplitudes saturate is of the order of $\tau \approx 1/\epsilon$. If, on the other hand, the nonlinearity is not confining, the amplitudes will grow rapidly until they are saturated by higher order nonlinearities.

Since we are looking for period-2 solutions close to onset, we will assume that the nonlinearity is confining and the mode amplitudes saturate to give a stable period-2 periodic state. At saturation, $a_n(\mathbf{k})$ can be expressed as $a_n(\mathbf{k}) = (-1)^n c(\mathbf{k}) + d(\mathbf{k})$. This suggests that we describe the amplitude $a_n(\mathbf{k}_1)$ with $|\mathbf{k}_1| = k_0$ for all n by

$$a_n(\mathbf{k}_1) = (-1)^n c_n(\mathbf{k}_1) + d_n(\mathbf{k}_1), \tag{20}$$

where the amplitudes c_n and d_n depend on the slow time scale ϵn, that is, they only vary on time scales of the order of $\tau = 1/\epsilon$.

We will now look at the modes with $\big||\mathbf{k}| - k_0\big| > 1/l$. Equation (14) implies that $\alpha(\mathbf{k}) \geqslant -1 + \mu$ for this case. If $\alpha > -1+\mu$ with $0 < \mu < 1$, $|\alpha|^p \ll 1$ for $p \geqslant 1/\mu$. Therefore, for long times n, the solution a_n in Eq. (19) relaxes on a time scale shorter than $1/\mu$, and is essentially determined by the inhomogeneous (forcing) term f_m for $n - \mu^{-1} < m < n$.

Note that, sufficiently close to onset, the time scale μ^{-1} is much smaller than τ. Consequently, Eq. (20) show that the amplitudes c and d are essentially constant over the time scales on which the mode amplitudes $a_n(\mathbf{k})$ with $\big||\mathbf{k}| - k_0\big| > 1/l$ evolve. Also, note that a, the amplitude of the modes with $|\mathbf{k}| = k_0$, is given by $a \sim \epsilon^{1/(p-1)}$ and this is small close to onset. Therefore, we can expand all the mode amplitudes in powers of ϵ and, close to onset, it suffices to keep the term with the smallest power.

We will now formally carry out this procedure of keeping the terms with the smallest powers of ϵ in the evolution of each mode $a_n(\mathbf{k})$. Let $C_1 \subseteq C$ denote the set of all the modes $\mathbf{k}_m \in C$ with $|\mathbf{k}_m| = k_0$. Then $\mathbf{k} \in C_1$ implies that $-\mathbf{k} \in C_1$. Also, let $C_2 \subseteq C$ denote the set of all the modes $\mathbf{k}_m \in C - C_1$ with $I_b(\mathbf{k}_i + \mathbf{k}_j - \mathbf{k}_m) = 1$, where $\mathbf{k}_i$, $\mathbf{k}_j \in C_1$. $\mathbf{k} \in C_2$ implies that $-\mathbf{k} \in C_2$. For the modes in C_2, to the lowest order in the mode amplitudes of the modes in C_1 [Eq. (16)] gives,

$$a_{n+1}(\mathbf{k}) = \alpha(\mathbf{k}) a_n(\mathbf{k}) + \beta \overline{f}(|\mathbf{k}|) \times \sum_{\mathbf{k}_1} \sum_{\mathbf{k}_2} I_b(\mathbf{k}_1 + \mathbf{k}_2 - \mathbf{k}) a_n(\mathbf{k}_1) a_n(\mathbf{k}_2),$$

where the summations are now restricted to $\mathbf{k}_1 \in C_1$ and $\mathbf{k}_2 \in C_1$. From the discussion above, the mode amplitudes $a_n(\mathbf{k}_i)$ for $\mathbf{k}_i \in C_1$ vary on time scales much longer than the time scale $[1 - |\alpha(\mathbf{k})|]^{-1}$ for $\mathbf{k} \in C_2$. Therefore, using the expression in Eq. (20), we can solve the above difference equation to obtain

$$a_n(\mathbf{k}) = \beta \overline{f}(|\mathbf{k}|) \sum_{\mathbf{k}_1} \sum_{\mathbf{k}_2} I_b(\mathbf{k}_1 + \mathbf{k}_2 - \mathbf{k}) \times \left(\frac{c_n(\mathbf{k}_1) c_n(\mathbf{k}_2) + d_n(\mathbf{k}_1) d_n(\mathbf{k}_2)}{1 - \alpha(\mathbf{k})} + \frac{(-1)^n [c_n(\mathbf{k}_1) d_n(\mathbf{k}_2) + d_n(\mathbf{k}_1) c_n(\mathbf{k}_2)]}{1 + \alpha(\mathbf{k})} \right).$$

Since $\alpha(\mathbf{k}) = \lambda(r) f(|\mathbf{k}|)$, only depends on $|\mathbf{k}|$, we can simplify the above expression by defining

$$\overline{g}_{\pm}(k) = \frac{\beta \overline{f}(k)}{1 \pm \lambda(r) \overline{f}(k)}.$$

With these definitions, we have

$$a_n(\mathbf{k}) = \sum_{k_1} \sum_{k_2} I_b(\mathbf{k}_1 + \mathbf{k}_2 - \mathbf{k}) \times \{ \overline{g}_-[(|\mathbf{k}|)(c_n(\mathbf{k}_1) c_n(\mathbf{k}_2) + d_n(\mathbf{k}_1) d_n(\mathbf{k}_2)] + (-1)^n \overline{g}_+(|\mathbf{k}|)[c_n(\mathbf{k}_1) d_n(\mathbf{k}_2) + d_n(\mathbf{k}_1) c_n(\mathbf{k}_2)] \}. \tag{21}$$

Note the following features about the solution for the mode amplitudes $a_n(\mathbf{k})$ for $\mathbf{k} \in C_2$ given by Eq. (21).

(1) The mode amplitudes $a_n(\mathbf{k})$ for $\mathbf{k} \in C_2$ are completely determined by the amplitudes for the wave vectors in C_1, that is they are *slaved* to the amplitudes $a_n(\mathbf{k}_i)$ for $\mathbf{k}_i \in C_1$.

(2) If c, $d \sim \epsilon^{1/(p-1)}$, for all $\mathbf{k} \in C_2$, we have $a_n(\mathbf{k}) \sim (c^2 + d^2) \sim \epsilon^{2/(p-1)}$. Therefore, the mode amplitudes for $\mathbf{k} \in C_2$ are higher order in ϵ than the mode amplitudes of the wave vectors in C_1.

(3) If c_n and d_n saturate to constant values, the mode amplitudes for all $\mathbf{k} \in C_2$ saturate to a period-2 state.

We can extend the above construction as follows. If $\mathbf{k} \in C$, we define $\deg(\mathbf{k})$ to be the smallest integer m such that (1) $m_1, m_2, \ldots, m_q$ are positive integers with

$$m_1 + m_2 + \cdots + m_q = m,$$

and (2) there exist wave vectors $\mathbf{k}_1, \mathbf{k}_2, \ldots, \mathbf{k}_q \in C_1$ such that

$$I_b(m_1 \mathbf{k}_1 + m_2 \mathbf{k}_2 + \cdots + m_q \mathbf{k}_q - \mathbf{k}) = 1.$$

A similar analysis to the one carried out above will show that if $\deg(\mathbf{k})=m\geqslant 3$, the mode amplitude $a_n(\mathbf{k})$ is completely determined by the mode amplitudes of the modes in C_1, it is of a higher order in ϵ with $a_n(\mathbf{k})\sim\epsilon^{m/(p-1)}$, and it will asymptote to a period-2 solution if the mode amplitudes in C_1 do so. Note that this justifies the claim that we made at the beginning of this section, that the modes with the largest amplitudes have $|\mathbf{k}|=k_0$. To solve for the mode amplitudes of the modes in C_1, we will substitute the expressions in Eq. (21) in Eq. (16) with $\mathbf{k}\in C_1$, keep the linear terms as well as the terms that are the lowest order in the nonlinearity, and solve the resulting equations for the mode amplitudes.

We have now reduced the problem of finding the pattern selected in the nonlinear regime to an appropriate specification of the set C_1, and to solving Eq. (16) for the amplitudes of these modes. In the rest of this section, we will consider various choices for C_1, and we will work out the pattern selection in each case.

A. Single dominant mode

We first consider the simplest case, namely, that of a single dominant mode $\mathbf{k}$, so that $C_1=\{\mathbf{k},-\mathbf{k}\}$. In this case, we can suppress the dependence on $\mathbf{k}$ and define $c_n=c_n(k)$, $d_n=d_n(\mathbf{k})$. Then, Eq. (20) along with the fact that ξ is real gives

$$a_n(\mathbf{k})=(-1)^n c_n+d_n,\quad a_n(-\mathbf{k})=(-1)^n c_n^*+d_n^*.$$

Using these expressions in Eq. (21) yields

$$\begin{aligned}a_n(\mathbf{0})&=2\overline{g}_-(0)(|c_n|^2+|d_n|^2)\\&\quad+2(-1)^n\overline{g}_+(0)(c_n d_n^*+d_n c_n^*),\\ a_n(2\mathbf{k})&=\overline{g}_-(2k_0)(c_n^2+d_n^2)+2(-1)^n\overline{g}_+(0)c_n d_n,\qquad(22)\\ a_n(-2\mathbf{k})&=\overline{g}_-(2k_0)((c_n^*)^2+(d_n^*)^2)+2(-1)^n\overline{g}_+(0)c_n^* d_n^*,\end{aligned}$$

From Eq. (16), we obtain

$$\begin{aligned}a_{n+1}(\mathbf{k})&=-(1+\epsilon)a_n(\mathbf{k})+2\beta\overline{f}(k_0)a_n(\mathbf{0})a_n(\mathbf{k})\\&\quad+2\beta\overline{f}(k_0)a_n(2\mathbf{k})a_n^*(\mathbf{k})+3\gamma|a_n(\mathbf{k})|^2a_n(\mathbf{k}),\end{aligned}\qquad(23)$$

where we have kept all terms up to order $a_n(\mathbf{k})^3$. Using the expressions in Eq. (22) in Eq. (23), and collecting all the terms that have a time dependence of the form $(-1)^n$, we obtain

$$\begin{aligned}c_{n+1}&=(1+\epsilon)c_n-2\beta\overline{f}(k_0)[2\overline{g}_-(0)(|c_n|^2c_n+|d_n|^2c_n)\\&\quad+\overline{g}_-(2k_0)(|c_n|^2c_n+|d_n|^2c_n^*)+2\overline{g}_+(0)\\&\quad\times(|d_n|^2c_n+d_n^2c_n^*)+2\overline{g}_+(2k_0)c_n|d_n|^2]\\&\quad+3\gamma(|c_n|^2c_n+2|d_n|^2c_n+d_n^2c_n^*).\end{aligned}\qquad(24)$$

This equation can be written

$$c_{n+1}-c_n=\epsilon c_n+N(c_n,d_n),$$

where the nonlinear term is homogeneous of degree 3, so that $N\sim a^p$ with $p=3$. It is clear that in the initial stages, c_n grows exponentially on the time scale ϵn. If the nonlinearity is confining, we see that the amplitude for c will saturate at $c\sim e^{1/(p-1)}=\epsilon^{1/2}$.

Using the expressions in Eq. (22) in Eq. (16), and collecting all the terms without a time dependence of the form $(-1)^n$, we obtain

$$d_{n+1}=-(1+\epsilon)d_n+N'(c_n,d_n),$$

where the nonlinearity is again homogeneous of degree 3. Note that, in this case, there is no nonzero solution of this equation that evolves on the slow time scale ϵn. Another way to see this is to note that there are no solutions for $d_{n+1}=d_n$ with $d\sim\epsilon^{1/2}$ and any such solution will have $d_n\sim O(1)$. Therefore, if the nonlinearity is confining, the only consistent solution is $d_n=0$.

If we derive the equation for d_n on the slow scale ϵn rigorously using an averaging procedure and the appropriate solvability conditions [34], we obtain

$$d_{n+1}=\frac{N'(c_n,d_n)}{2}$$

for all n and $d_0=0$. Since $N'(c,d)=0$ for $d=0$, it follows that $d_n=0$ for all n. Using this, and defining ν_s by

$$\nu_s=2\beta\overline{f}(k_0)[2\overline{g}_-(0)+\overline{g}_-(2k_0)]-3\gamma.\qquad(25)$$

we can rewrite Eq. (24) as

$$c_{n+1}=(1+\epsilon)c_n-\nu_s|c_n|^2c_n.$$

If $\nu_s>0$, we see that c_n will grow until it saturates at

$$c_n h_{\mathrm{st}}=\left(\frac{\epsilon}{\nu_s}\right)^{1/2}e^{i\phi},$$

where $\phi=\arg(c_0)$ is an arbitrary phase angle. Note that the amplitude has the expected $\epsilon^{1/2}$ behavior. Linearizing about $c=h_{\mathrm{st}}$ we see that

$$c_{n+1}=(1-2\epsilon)c_n+2\epsilon h_{\mathrm{st}}$$

Therefore, for $\epsilon<1/2$ the fixed point $c_n=h_{\mathrm{st}}$ is stable. Further, the solution c_n relaxes to this value exponentially on a time scale $1/(2\epsilon)\sim\tau$, justifying our earlier claim that the dynamics of the mode amplitude $a_n(\mathbf{k})$ is on a time scale τ over both the growth stage and the saturation stage.

The periodic pattern corresponding to this solution is a period-2 stripe given by

$$\xi_n(\mathbf{x})=\xi_*+(-1)^n\left(\frac{\epsilon}{\nu_s}\right)^{1/2}[e^{i(\mathbf{k}\cdot\mathbf{x}+\phi)}+e^{-i(\mathbf{k}\cdot\mathbf{x}+\phi)}]+O(\epsilon).\qquad(26)$$

We will conclude our discussion of the case of a single dominant mode with a few remarks.

(1) From Eqs. (23) and (22), we see that $a_n(\mathbf{k}) \to -a_n(\mathbf{k})$, $a_n(\mathbf{0}) \to a_n(\mathbf{0})$, and $a_n(2\mathbf{k}) \to a_n(2\mathbf{k})$ are exact symmetries of this system of equations to this order. In fact, if we set $C=\{n\mathbf{k}|n\in\mathbb{Z}\}$ and expand the map to arbitrary orders in $\xi - \xi_*$ [cf. Eq. (15)], we can show that

$$a_n(\mathbf{k}_1) \to (-1)^{\deg(\mathbf{k}_1)} a_n(\mathbf{k}_1)$$

is an exact symmetry of the system.

(2) Combining the above symmetry along with the discrete time translation symmetry $a_n(\mathbf{k}_1) \to a_{n+1}(\mathbf{k}_1)$, we see that an exact symmetry of the system is

$$c_n(\mathbf{k}_1) \to (-1)^{\deg(\mathbf{k}_1)+1} c_n(\mathbf{k}_1),$$

$$d_n(\mathbf{k}_1) \to (-1)^{\deg(\mathbf{k}_1)} d_n(\mathbf{k}_1).$$

If the nonlinearity is confining, so that we expect a solution with small amplitudes as $\epsilon \to 0$, then the solution is invariant under the above transformation, that is $c_n(\mathbf{k}_1)=0$ if $\deg(k_1)$ is even and $d_n(\mathbf{k}_1)=0$ if $\deg(\mathbf{k}_1)$ is odd. It is also true that any solution that evolves from an initial state that is close to a spatially homogeneous state will have these properties.

(3) The symmetries noted in remarks (1) and (2) above are a reflection of the fact that, for $C=\{n\mathbf{k}|n\in\mathbb{Z}\}$,

$$I_b(m_1\mathbf{k}_1 \pm m_2\mathbf{k}_2 \pm \cdots \pm m_q\mathbf{k}_q)=1,$$

with $\mathbf{k}_1,\mathbf{k}_2,\ldots,\mathbf{k}_q \in C$, implies that

$$m_1 \deg(\mathbf{k}_1) + m_2 \deg(k_2) + \cdots + m_q \deg(\mathbf{k}_q)$$

is even. This, along with Eq. (16) directly implies the claims in remark (1).

(4) The lowest order of the nonlinearities in Eq. (23) coming from the terms with $a_n(\mathbf{0})$ and $a_n(2\mathbf{k})$ is $a_n(\mathbf{k})^3$. Consequently, in order to keep consistency and retain all terms of this order, we have to expand the nonlinear map in Eq. (15) to the third order.

(5) The explicit form of the stripe solution in Eq. (26) displays the time and space translation invariances, the rotational invariance, and the invariance under reflections of the set of all stripe solutions. We can use the translation invariance to choose a solution where $\phi=0$, so that c is real.

B. Two dominant modes

We now consider the case where there are two dominant modes $\mathbf{k}_1$ and $\mathbf{k}_2$ so that $C_1=\{\mathbf{k}_1,\mathbf{k}_2,-\mathbf{k}_1,-\mathbf{k}_2\}$. In this case, we have $C=\{m_1\mathbf{k}_1+m_2\mathbf{k}_2|m_1,m_2\in\mathbb{Z}\}$.

Due to the symmetries of the system under rotations and reflections, we have the freedom to relabel $\mathbf{k}_2$ as $-\mathbf{k}_2$. Therefore, we can always choose $\mathbf{k}_1$ and $\mathbf{k}_2$ such that $\theta = \cos^{-1}(|\mathbf{k}_1\cdot\mathbf{k}_2|/k_0^2)$ is in the range $[0,\pi/2]$. By the symmetries of the system, C is completely characterized by the angle θ.

For the two dominant modes assumption to be consistent, we need that $||m_1\mathbf{k}_1+m_2\mathbf{k}_2|-k_0|>1/l$ unless $|m_1|+|m_2|=1$. This will be true for $\theta\in[\pi/3+2/l,\pi/2]$, and we will always choose θ in this range.

If θ is chosen in this range, C has the property that

$$I_b(m_1\mathbf{k}_1 \pm m_2\mathbf{k}_2 \pm \cdots \pm m_q\mathbf{k}_q)=1.$$

$\mathbf{k}_1,\mathbf{k}_2,\ldots,\mathbf{k}_q \in C$ implies that

$$m_1\deg(k_1) + m_2\deg(k_2) + \cdots + m_q\deg(k_q)$$

is even. As in Sec. IX A, this implies that

$$a_n(\mathbf{k}) = (-1)^n c_n(\mathbf{k})$$

if $\deg(\mathbf{k})$ is odd, and

$$a_n(\mathbf{k}) = d_n(\mathbf{k})$$

if $\deg(\mathbf{k})$ is even, for a solution that evolves from an initial condition that is close to being spatially homogeneous.

For $C_1=\{\mathbf{k}_1,\mathbf{k}_2,-\mathbf{k}_1,-\mathbf{k}_2\}$ and $C_2=\{\mathbf{0},\mathbf{k}_1+\mathbf{k}_2,\mathbf{k}_1-\mathbf{k}_2,-\mathbf{k}_1-\mathbf{k}_2,-\mathbf{k}_1+\mathbf{k}_2,2\mathbf{k}_1,2\mathbf{k}_2,-2\mathbf{k}_1,-2\mathbf{k}_2\}$, Eq. (21) yields

$$\begin{aligned}
a_n(\mathbf{0}) &= 2\overline{g}_-(0)[|c_n(\mathbf{k}_1)|^2|c_n(\mathbf{k}_2)|^2],\\
a_n(\mathbf{k}_1+\mathbf{k}_2) &= 2\overline{g}_-[2k_0\cos(\theta/2)]c_n(\mathbf{k}_1)c_n(\mathbf{k}_2),\\
a_n(\mathbf{k}_1-\mathbf{k}_2) &= 2\overline{g}_-[2k_0\sin(\theta/2)]c_n(\mathbf{k}_1)c_n^*(\mathbf{k}_2),\\
a_n(2\mathbf{k}_1) &= \overline{g}_-(2k_0)c_n^2(\mathbf{k}_1),\\
a_n(2\mathbf{k}_2) &= \overline{g}_-(2k_0)c_n^2(\mathbf{k}_2),
\end{aligned} \tag{27}$$

and the amplitudes of the other modes in C_2 are obtained by complex conjugating the appropriate expression from the list above. From Eq. (16), we obtain

$$\begin{aligned}
a_{n+1}(\mathbf{k}_1) = &-(1+\epsilon)a_n(\mathbf{k}_1) + 2\beta\overline{f}(k_0)[a_n(\mathbf{0})a_n(\mathbf{k}_1)\\
&+ a_n(2\mathbf{k}_1)a_n^*(\mathbf{k}_1) + a_n(\mathbf{k}_1+\mathbf{k}_2)a_n^*(\mathbf{k}_2)\\
&+ a_n(\mathbf{k}_1-\mathbf{k}_2)a_n(\mathbf{k}_2)] + 3\gamma|a_n(\mathbf{k}_1)|^2 a_n(\mathbf{k}_1),\\
a_{n+1}(\mathbf{k}_2) = &-(1+\epsilon)a_n(\mathbf{k}_2) + 2\beta\overline{f}(k_0)[a_n(\mathbf{0})a_n(\mathbf{k}_2)\\
&+ a_n(2\mathbf{k}_2)a_n^*(k_2) + a_n(\mathbf{k}_2+\mathbf{k}_1)a_n^*(\mathbf{k}_1)\\
&+ a_n(\mathbf{k}_2-\mathbf{k}_1)a_n(\mathbf{k}_1)] + 3\gamma|a_n(\mathbf{k}_2)|^2 a_n(\mathbf{k}_2),
\end{aligned} \tag{28}$$

where we retain all terms up to order $\max[|a_n(\mathbf{k}_1)|,|a_n(\mathbf{k}_2)|]^3$.

Define ν_c by

$$\begin{aligned}
\nu_c = 4\beta\overline{f}(k_0)\{&\overline{g}_-(0) + \overline{g}_-[2k_0\sin(\theta/2)]\\
&+ \overline{g}_-[2k_0\cos(\theta/2)]\}.
\end{aligned} \tag{29}$$

Note that ν_c is a function of θ. Using this definition, the definition of ν_s in Eq. (25), the fact that $a_n(k_i) = (-1)^n c_n(k_i)$ for $i=1$ and 2, and simplifying the results of substituting Eq. (27) into Eq. (28), we obtain

$$\begin{aligned}
c_{n+1}(\mathbf{k}_1) = (1+\epsilon)c_n(\mathbf{k}_1) - [&\nu_s|c_n(\mathbf{k}_1)|^2\\
&+ \nu_c|c_n(\mathbf{k}_2)|^2]c_n(\mathbf{k}_1).
\end{aligned}$$

The equation for $c_n(\mathbf{k}_2)$ is obtained from the above equation by the symmetry transformations $\mathbf{k}_1 \to \mathbf{k}_2$ and $\mathbf{k}_2 \to \mathbf{k}_1$. To simplify the notation, we set $x_n = c_n(\mathbf{k}_1)e^{-i\phi_1}$ and $y_n = c_n(\mathbf{k}_2)e^{-i\phi_2}$, where $\phi_1 = \arg[c_0(\mathbf{k}_1)]$ and $\phi_2 = \arg[c_0(\mathbf{k}_2)]$. x_n and y_n are real for all n, and they obey the equations

$$\begin{aligned} x_{n+1} &= (1+\epsilon)x_n - (\nu_s x_n^2 + \nu_c y_n^2)x_n, \\ y_{n+1} &= (1+\epsilon)y_n - (\nu_s y_n^2 + \nu_c x_n^2)y_n. \end{aligned} \tag{30}$$

If $\nu_s > 0$, $\nu_s + \nu_c > 0$, the amplitudes x_n and y_n will grow on the slow scale ϵn and then saturate.

We will first determine all the fixed point of the system in Eq. (30). The fixed points of the system for $\nu_c \neq \nu_s$ are the origin $(x,y) = (0,0)$, the *stripe solutions*

$$(x,y) = (\pm h_{\rm st}, 0), \quad (x,y) = (0, \pm h_{\rm st}),$$

and the *rhombus solutions*

$$(x,y) = (\pm h_{\rm rh} \pm h_{\rm rh}),$$

where

$$h_{\rm rh} = \left(\frac{\epsilon}{\nu_c + \nu_s} \right)^{1/2}.$$

If $\nu_c = \nu_s$, the fixed points are the origin (0, 0) and all the points on the circle

$$x^2 + y^2 = \frac{\epsilon}{\nu_s} = \frac{2\epsilon}{\nu_s + \nu_c}.$$

The fixed point at (0, 0) has two unstable directions. Setting $y_0 = 0$ will bring us back to the case of one dominant mode, which was considered in Sec. (IX A). In this case, $y_n = 0$ for all n showing that $y = 0$ is an invariant manifold for the dynamics. From the discussion in Sec. IX A, we know that the solution converges to the stripe solution that is given by a fixed point where $x = h_{\rm st}$ and $y = 0$. We can now check for the stability of this state to perturbations which introduce a second mode. Linearizing about this fixed point, we obtain

$$\delta x_{n+1} = (1 - 2\epsilon)\delta x_n,$$

$$\delta y_{n+1} = \left(1 + \epsilon \frac{\nu_s - \nu_c}{\nu_s} \right) \delta y_n,$$

Consequently, the stripe solution is stable to the introduction of a second mode if $\nu_c / \nu_s > 1$. Also, as we vary the parameters, it will first become unstable to a mode corresponding to the angle θ with the smallest value of ν_c / ν_s. The eigenvalue for perturbations in the direction $\delta y_n = 0$ is $\lambda_s = 1 - 2\epsilon$, and the eigenvalue corresponding to the direction $\delta x_n = 0$ is given by

$$\lambda_1 = \left(1 + \epsilon \frac{\nu_s - \nu_c}{\nu_s} \right)$$

We can also look at solutions with $x_0 = y_0$. These solutions have $x_n = y_n$ for all n, so that the line $x = y$ is also an invariant manifold for the system. The evolution of x_n is then given by

$$x_{n+1} = (1+\epsilon)x_n - (\nu_s + \nu_c)x_n^3.$$

If $\nu_c + \nu_s > 0$, the amplitudes will grow and saturate at

$$x = y = h_{\rm rh} = \left(\frac{\epsilon}{\nu_s + \nu_c} \right)^{1/2}.$$

We can check for the stability of this state to perturbations which make $x_n \neq y_n$. Linearizing about this fixed point, we obtain

$$\delta x_{n+1} = \left(1 - \frac{2\nu_s \epsilon}{\nu_s + \nu_c} \right) \delta x_n - \frac{2\nu_c \epsilon}{\nu_s + \nu_c} \delta y_n,$$

$$\delta y_{n+1} = \left(1 - \frac{2\nu_s \epsilon}{\nu_s + \nu_c} \right) \delta y_n - \frac{2\nu_c \epsilon}{\nu_s + \nu_c} \delta x_n.$$

From this, we see that this fixed point has an eigendirection $\delta y_n = -\delta x_n$ yielding the eigenvalue

$$\lambda_2 = \left(1 + 2\epsilon \frac{\nu_c - \nu_s}{\nu_c + \nu_s} \right).$$

This yields instability (stability) if $\nu_c > \nu_s$ ($\nu_c < \nu_s$). The eigenvalue corresponding to the direction $\delta y_n = \delta x_n$ is $\lambda_s = 1 - 2\epsilon$, so that the fixed point is always stable to perturbations with $\delta x = \delta y$.

Finally, we consider the circle of fixed points in the case $\nu_s = \nu_c$. In this case, $x_0 = p y_0$ implies that $x_n = p y_n$ for all n and all p. Therefore, all the rays $x = py$ are invariant under the dynamics. The evolution of x_n is given by

$$\begin{aligned} x_{n+1} &= (1+\epsilon)x_n - (\nu_s + p^{-2}\nu_c)x_n^3 \\ &= (1+\epsilon)x_n - (1+p^{-2})\nu_s x_n^3. \end{aligned}$$

The amplitudes will therefore grow and saturate at

$$x = py = p\left(\frac{\epsilon}{(1+p^2)\nu_s} \right)^{1/2},$$

In this case, the circle of fixed points are stable to perturbations that move (x,y) off the circle, i.e., perturbations in the direction $\delta x_n = p\,\delta y_n$ with an eigenvalue $\lambda_s = 1 - 2\epsilon$, but the direction $\delta y_n = -p\,\delta x_n$ along the circle is a neutral direction.

We summarize the results of this analysis in the phase portraits in Fig. 12. Figure 12(a) depicts the dynamics for the case $\nu_s = \nu_c$. The circle of fixed points is an invariant manifold for the dynamics. If $\epsilon < 1/2$, the eigenvalue in the stable direction $\lambda_s = 1 - 2\epsilon > 0$. In this case, points that start out inside the circle of fixed points remain inside it on iterating the in Eq. (30). x_n and y_n increase monotonically and saturate at the fixed point $x = py = p\sqrt{\epsilon/[(1+p^2)\nu_s]}$, where $p = x_0/y_0$, and the corresponding pattern is given by

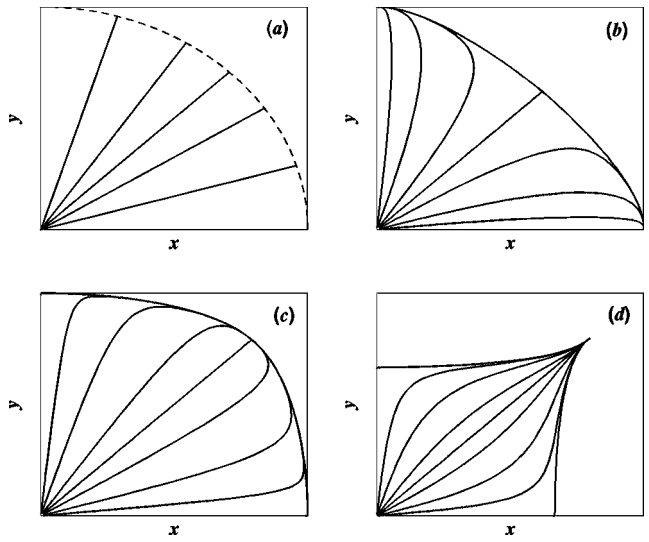

FIG. 12. Schematic phase portraits for the system in Eq. (30) in various parameter regimes. (a) $\nu_s=\nu_c$. (b) $\nu_s<\nu_c$. (c) $\nu_s>\nu_c>0$. (d) $-\nu_s<\nu_c<0$. The dashed line in (a) is a circle of fixed points.

$$\xi_n(\mathbf{x})=\xi_*+(-1)^n\left(\frac{\epsilon}{\nu_s[|c_0(\mathbf{k}_1)|^2+|c_0(\mathbf{k}_2)|^2]}\right)^{1/2}\times[c_0(\mathbf{k}_1)e^{i\mathbf{k}_1\cdot\mathbf{x}}+c_0^*(\mathbf{k}_1)e^{-i\mathbf{k}_1\cdot\mathbf{x}}+c_0(\mathbf{k}_2)e^{i\mathbf{k}_2\cdot\mathbf{x}}+c_0^*(\mathbf{k}_2)e^{-i\mathbf{k}_2\cdot\mathbf{x}}]+O(\epsilon). \tag{31}$$

The circle of fixed points for the case $\nu_s=\nu_c$ persists as an invariant manifold even when $\nu_c\neq\nu_s$. It now becomes orbits connecting the stripe solutions $(x,y)=(\pm h_{\rm st},0)$ and $(x,y)=(0,\pm h_{\rm st})$, with the rhombus solutions $(x,y)=(\pm h_{\rm rh},\pm h_{\rm rh})$. The eigenvalues for the linearization near the stripe solution are $\lambda_s=1-2\epsilon$ and $\lambda_1=1+\epsilon(\nu_s-\nu_c)/\nu_s$. The eigenvalues for the linearization near the rhombus solution are $\lambda_s=1-2\epsilon$ and $\lambda_1=1+2\epsilon(\nu_c-\nu_s)/(\nu_c+\nu_s)$.

Figure 12(b) depicts the dynamics for the case $\nu_s<\nu_c$. For sufficiently small $\epsilon<1/2$ and $\nu_s<\nu_c$, we have $0<\lambda_s<1$, $0<\lambda_1<1$, and $\lambda_2>1$. The stripe solution is therefore stable, and the rhombus solution has one unstable direction. Since all the eigenvalues are positive, the map in Eq. (30) maps regions bounded by invariant curves into themselves. In Fig. 12(b), we show the region bounded by the invariant curves $x=0$ and $y=0$ and the unstable manifold of the rhombus solution $x=y=h_{\rm rh}$. It is clear that all initial conditions such that $x_0>y_0>0$ lead to solutions that asymptote to $x=h_{\rm st}$ and $y=0$. Similarly, initial conditions $y_0>x_0>0$ lead to solutions that asymptote to $y=h_{\rm st}$ and $x=0$. The asymptotic pattern is a stripe pattern and it is described by Eq. (26).

Figure 12(c) is the phase portrait when $\nu_s>\nu_c>0$, and Fig. 12(d) is the phase portrait for $\nu_c<0$, $\nu_s+\nu_c>0$. For sufficiently small $\epsilon<1/2$ and $\nu_s>\nu_c$, we have $0<\lambda_s<1$, $\lambda_1>1$, and $0<\lambda_2<1$. The stripe solution is unstable to the rhombus solution in both these regimes. All the eigenvalues are again positive and regions bounded by invariant curves map into themselves by Eq. (30). Figures 12(c) and 12(d), show the region bounded by the invariant curves $x=0$ and $y=0$, and pieces of the unstable manifolds of the stripe solutions $x=h_{\rm rh}$, $y=0$, and $x=0$, $y=h_{\rm rh}$. In this case, all initial conditions $x_0>0$ and $y_0>0$, with x_0 and y_0 small, lead to solutions that saturate at $x=y=h_{\rm rh}$. The rhombus solution is given by

$$\xi_n(\mathbf{x})=\xi_*+(-1)^n\left(\frac{\epsilon}{\nu_s+\nu_c}\right)^{1/2}[e^{i(\mathbf{k}_1\cdot\mathbf{x}+\phi_1)}+e^{-i(\mathbf{k}_1\cdot\mathbf{x}+\phi)}+e^{i(\mathbf{k}_2\cdot\mathbf{x}+\phi_2)}+e^{-i(\mathbf{k}_2\cdot\mathbf{x}+\phi_2)}]+O(\epsilon), \tag{32}$$

where $\phi_1=\arg[c_0(\mathbf{k}_1)]$ and $\phi_2=\arg[c_0(\mathbf{k}_2)]$, as defined above. The difference between the regimes $0<\nu_c<\nu_s$ and $-\nu_s<\nu_c<0$ are in the transient growth stage and we will consider this below.

In our discussion up to this point, we have assumed that the angle θ, which determines C, has been given. In order to completely describe the patterns with two dominant modes, we therefore need to consider the question of what factors determine the angle θ. In this connection, we will make the following observations.

(1) When the stripe state goes unstable on varying parameters, an instability occurs when ν_s crosses from from $\nu_s<\nu_c$ to $\nu_s>\nu_c$. Consequently, the first additional mode that goes unstable corresponds to a θ with the smallest value of ν_c.

(2) From the dynamics in Eq. (30), we see that

$$x_{n+1}=(1+\epsilon-\nu_s x_n^2-\nu_c y_n^2)x_n,$$

and a similar equation is obeyed by y_n. In the initial stage, where x_n and y_n are much smaller than $O(\sqrt{\epsilon})$, the initial growth rate is $1+\epsilon$, independent of ν_c and consequently of θ. However, once the modes grow so that $x_n, y_n\sim O(\sqrt{\epsilon})$, it is clear that the mode with the largest ''nonlinear'' growth rate is the one for which ν_c takes on its smallest possible value. Consequently, if we start from an initial state that is a small random perturbation of a spatially uniform state and we are in a parameter regime where $\nu_s>\nu_c$, so that the rhombus solution is stable, we expect that the dynamics will select a rhombus solution with wave vectors $\mathbf{k}_1$ and $\mathbf{k}_2$ such that the angle θ minimizes ν_c.

(3) In a parameter regime where $0<\nu_c<\nu_s$, we see from Eq. (24) that the dynamics of a stripe pattern is given by

$$x_{n+1}=(1+\epsilon-\nu_s x_n^2)x_n.$$

Since $\nu_c>0$, the two preceding equations imply that the nonlinear growth rate for the stripe solution is larger than that of the rhombus solution. However, the parameters are such that the stripe is unstable. Therefore, in this regime, we expect an initial transient where the pattern evolves so that it looks like a stripe solution, i.e., $y_n\approx 0$ and x_n will increase and saturate. The solution will then evolves to the rhombus solution that is asymptotically stable. If, however, $\nu_c<0$, but $\nu_s>-\nu_c$ so that $\nu_s+\nu_c>0$, the nonlinear growth rate for the rhombus solution is larger. Therefore, in the initial transient growth,

the solution will look like a rhombus solution, i.e., the solution will quickly become $x_n \approx y_n$ after which both the modes will grow till they saturate.

(4) The preceding discussion invoking the concept of a ''nonlinear'' growth rate is not rigorous. However, in this case we can justify the conclusions rigorously. In the regime where the rhombus solution is stable, the eigenvalues for the linearized dynamics near the fixed point $(x,y)=(h_{rh},h_{rh})$ are $\lambda_s=1-2\epsilon$ and $\lambda_2=1-2\epsilon(\nu_s-\nu_c)/(\nu_s+\nu_c)$. Asymptotically, the solutions x_n and y_n will approach the fixed point along the direction corresponding to the less stable (larger) eigenvalue. Consequently, for $\nu_c>0$, $\lambda_s<\lambda_2$, so that the solutions approach the fixed point along the eigendirection corresponding to λ_2, the unstable manifold of the stripe solution. Therefore, the evolution of an arbitrary small initial condition will consist of a transient growth phase where the solution approaches the stripe fixed point as illustrated in Fig. 12(c). For $\nu_c<0$, $\lambda_2<\lambda_s$ and the solutions approach the fixed point along the invariant manifold $x=y$, as illustrated in Fig. 12(d), and there is no transient stripe.

From the above remarks, we expect that the value of θ selected corresponds to the smallest value of ν_c. From Eq. (29) it follows that ν_c is symmetric under $\theta\rightarrow\pi-\theta$, implying that

$$\frac{d\nu_c}{d\theta}=0$$

at $\theta=\pi/2$. Therefore, generically, there is a codimension zero set of parameter values such that ν_c attains its minimum at $\theta=\pi/2$, corresponding to the formation of square patterns. Hence we expect that there are typical systems for which square patterns form generically (i.e., without any fine tuning of parameters).

We conclude our discussion of patterns with two dominant modes by discussing the nature of the transition between nonzero amplitude stripes and squares (or in general rhombi) at $\nu_s=\nu_c$. In the context of the two mode description of both these patterns, away from onset, this transition is first order (discontinuous) since a state with one mode amplitude being zero (the stripe solution) goes to a state with both modes having equal and nonzero amplitudes (the square or rhombus solution). However, contrary to what one would expect for a first order transition, this transition is not hysteretic. Both stripe to square (rhombus) and square (rhombus) to stripe transitions occur at $\nu_s=\nu_c$. This is a consequence of the existence of a continuous family of intermediate solutions (the circle of fixed points at $\nu_s=\nu_c$) connecting the stripe and the square (rhombus) solutions.

Although the transition is nonhysteretic, if we look at asymptotic states it will be effectively hysteretic if we only look at the evolution of the system for finite time intervals. For $\nu_s>\nu_c$, where the stripe solution is unstable, the unstable eigenvalue is given by $\lambda_1=1+\epsilon(\nu_s-\nu_c)/\nu_s$. Also, for $\nu_s<\nu_c$, where the square (rhombus) solution is unstable, the unstable eigenvalue is $\lambda_2=1+2\epsilon(\nu_c-\nu_s)/(\nu_c+\nu_s)$. Therefore, the time for the transition between the two states is given by

$$\tau_L\sim\frac{1}{\lambda_u-1}\sim\frac{\nu}{\epsilon|\nu_s-\nu_c|},$$

where λ_u is the relevant unstable eigenvalue and $\nu=(\nu_s+\nu_c)/2\approx\nu_s\approx\nu_c$ near the transition. Consequently, if we evolve the solution for a finite time T and $T\ll\tau_L$, we will be in a regime where both the stripe and the square (rhombus) solutions appear to be stable over this time scale. This explains why we see a region with coexisting squares and stripes in the phase diagram (Fig. 4). From the above considerations, it is clear that the width of this region in parameter space will decrease as the length of the run is increased and if p is a typical parameter, the width of the coexistence region Δp, is given by the requirement $T/\tau_L\sim 1$, and we therefore predict that Δp will scale with T, the length of the run, and the supercriticality ϵ as

$$\Delta p\sim|\nu_s-\nu|\sim\frac{|\nu_s-\nu_c|}{\nu}\sim(\epsilon T)^{-1}.$$

C. Hexagons near onset

To study hexagonal patterns, we consider the case of three dominant modes $\mathbf{k}_1$, $\mathbf{k}_2$, and $\mathbf{k}_3$, with $|\mathbf{k}_1|=|\mathbf{k}_2|=|\mathbf{k}_3|=k_0$, and the angles between any pair of these vectors being $2\pi/3$. This implies that

$$\mathbf{k}_1+\mathbf{k}_2+\mathbf{k}_3=\mathbf{0}.$$

In this case, $C_1=\{\mathbf{k}_1,\mathbf{k}_2,\mathbf{k}_3,-\mathbf{k}_1,-\mathbf{k}_2,-\mathbf{k}_3\}$. Since $\mathbf{k}_1+\mathbf{k}_2=-\mathbf{k}_3$ and $\deg(\mathbf{k}_1)=\deg(\mathbf{k}_2)=\deg(\mathbf{k}_3)=\mathbf{1}$,

$$I_b(m_1\mathbf{k}_1\pm m_2\mathbf{k}_2\pm\cdots\pm m_q\mathbf{k}_q)=1,$$

with $\mathbf{k}_1,\mathbf{k}_2,\ldots,\mathbf{k}_q\in C$, does not imply that

$$m_1\deg(\mathbf{k}_1)+m_2\deg(\mathbf{k}_2)+\cdots+m_q\deg(\mathbf{k}_q)$$

is even, in contrast to the cases with one or two dominant modes. Consequently, we can no longer assume that $a_n(\mathbf{k})=c_n(\mathbf{k})$ if $\deg(\mathbf{k})$ is odd and $a_n(\mathbf{k})=d_n(\mathbf{k})$ if $\deg(\mathbf{k})$ is even.

We have $C_2=\{\mathbf{0},\pm 2\mathbf{k}_1,\pm 2\mathbf{k}_2,\pm 2\mathbf{k}_3,\pm(\mathbf{k}_1-\mathbf{k}_2),\pm(\mathbf{k}_2-\mathbf{k}_3),\pm(\mathbf{k}_3-\mathbf{k}_1)\}$. We can obtain expressions for the amplitudes of the modes in C_2 using Eq. (21), and we do this in Appendix A. For our purposes, it suffices to consider the homogeneity and the symmetries of the expressions that are obtained [see Eq. (A1)]. If $\mathbf{q}\in C_2$, we have the following

(1) The lowest order terms in the expressions for $c_n(\mathbf{q})$ and $d_n(\mathbf{q})$ are quadratic in $\{c_n(\mathbf{k}_i),d_n(\mathbf{k}_i)\}$, $i\in\{1,2,3\}$ (the amplitudes of the modes in C_1).

(2) $d_n(\mathbf{q})$ is invariant under the transformation $d_n(\mathbf{k}_i)\rightarrow d_n(\mathbf{k}_i), c_n(\mathbf{k}_i)\rightarrow -c_n(\mathbf{k}_i)$, which is equivalent to saying that $d_n(\mathbf{q})$ is invariant (even) for time translations by one time step.

(3) $c_n(\mathbf{q})\rightarrow -c_n(\mathbf{q})$ under the transformation $d_n(\mathbf{k}_i)\rightarrow d_n(\mathbf{k}_i), c_n(\mathbf{k}_i)\rightarrow -c_n(\mathbf{k}_i)$, which is equivalent to saying that $c_n(\mathbf{q})$ changes sign (is odd) under time translations by one time step.

(4) If the amplitudes $\{c_n(\mathbf{k}_i), d_n(\mathbf{k}_i)\}$, $i \in \{1,2,3\}$ are real, $d_n(\mathbf{q})$ and $c_n(\mathbf{q})$ are also real.

From Eq. (16), we obtain

$$\begin{aligned} a_{n+1}(\mathbf{k}_1) = &-(1+\epsilon)a_n(\mathbf{k}_1) + 2\beta\overline{f}(k_0)[a_n^*(\mathbf{k}_2)a_n^*(\mathbf{k}_3) \\ &+ a_n(\mathbf{0})a_n(\mathbf{k}_1) + a_n(2\mathbf{k}_1)a_n^*(\mathbf{k}_1) \\ &+ a_n(\mathbf{k}_1-\mathbf{k}_2)a_n(\mathbf{k}_2) + a_n(\mathbf{k}_1-\mathbf{k}_3)a_n(\mathbf{k}_3)] \\ &+ 3\gamma|a_n(\mathbf{k}_1)|^2 a_n(\mathbf{k}_1), \end{aligned} \tag{33}$$

where we retain all terms up to order $\max[|a_n(\mathbf{k}_1)|, |a_n(\mathbf{k}_2)|, |a_n(\mathbf{k}_3)|]^3$. The expressions for $a_{n+1}(\mathbf{k}_2)$ and $a_{n+1}(\mathbf{k}_3)$ can be obtained from the above expression by cyclically permuting $\mathbf{k}_1$, $\mathbf{k}_2$, and $\mathbf{k}_3$. Note that the expression on the right hand side of Eq. (33) has a term $a_n^*(\mathbf{k}_2)a_n^*(\mathbf{k}_3)$ that is quadratic in the amplitudes of the modes in C_1, in contrast to the corresponding expressions for the case of one dominant mode in Eq. (23) and two dominant modes in Eq. (28), which are both cubic in the amplitudes of the modes in C_1.

We will look for fixed points corresponding to hexagonal patterns, that is, for solutions with $a_n(\mathbf{k}_1) = a_n(\mathbf{k}_2) = a_n(\mathbf{k}_3)$, $d_{n+1}(\mathbf{k}_1) = d_n(\mathbf{k}_1) = d$ and $c_{n+1}(\mathbf{k}_1) = -c_n(\mathbf{k}_1) = (-1)^{n+1}c$. Further, we will require that d and c are real, which is a consistent requirement, since if the amplitudes are real at time step n, they will stay real in the subsequent evolution. Substituting this ansatz in Eq. (33), and separating the terms with and without a time dependence of the form $(-1)^n$, we obtain

$$\begin{aligned} d &= -(1+\epsilon)d + 2\beta\overline{f}(k_0)(d^2+c^2) + N_e(c,d), \\ c &= (1+\epsilon)c - 4\beta\overline{f}(k_0)cd + N_o(c,d), \end{aligned} \tag{34}$$

where N_e and N_o are of degree 3 in $\{c,d\}$, N_e is even in $c[N_e(-c,d) = N_e(c,d)]$, and N_o is odd in $c[N_o(-c,d) = -N_o(c,d)]$.

From the first equation, we obtain

$$d = \frac{2\beta\overline{f}(k_0)(d^2+c^2) + N_e(c,d)}{2+\epsilon}.$$

Since we are looking for solutions such that $c,d \to 0$ as $\epsilon \to 0$, it follows that $d^2 \ll |d|$ for small ϵ. Also, $N_e(c,d)$ is of degree 3 and is even in c, so that $N_e(c,d) = (b_1 c^2 + b_2 d^2)d$ where b_1 and b_2 have $O(1)$ (finite) limits $\overline{b_1}$ and $\overline{b_2}$ as $\epsilon \to 0$. Consequently, for small ϵ, to lowest order we have

$$d = \beta\overline{f}(k_0)c^2.$$

Substituting this into the second equation, we have

$$c = (1+\epsilon)c - 4\beta^2[\overline{f}(k_0)]^2 c^3 + N_o(c,d).$$

Since $N_o(c,d)$ is of degree 3 and is odd in c, $N_o(c,d) = -(b_3 c^2 + b_4 d^2)c$, where b_3 and b_4 have $O(1)$ limits $\overline{b_3}$ and $\overline{b_4}$ as $\epsilon \to 0$. Since $d = O(c^2)$, to lowest order in ϵ, we have

$$\epsilon c = (4\beta^2[\overline{f}(k_0)]^2 + \overline{b_3})c^3,$$

so that

$$c = \left(\frac{\epsilon}{4\beta^2[\overline{f}(k_0)]^2 + \overline{b_3}} \right)^{1/2}$$

and

$$d = \frac{\beta\overline{f}(k_0)\epsilon}{4\beta^2[\overline{f}(k_0)]^2 + \overline{b_3}}.$$

We will now look at the dynamics of patterns with three modes, that are described by Eq. (33). Based on the above analysis, we will assume that the amplitudes a_n are real, and that $c_n \sim O(\sqrt{\epsilon})$ and $d_n \sim O(\epsilon)$. Using this ansatz in Eqs. (33) and (A1), keeping terms to the lowest order in ϵ, and looking for solutions that evolve on the slow scale ϵn, we obtain the equations

$$\begin{aligned} d_{n+1}(\mathbf{k}_1) &= \beta\overline{f}(k_0)c_n(\mathbf{k}_2)c_n(\mathbf{k}_3), \\ c_{n+1}(\mathbf{k}_1) &= (1+\epsilon)c_n(\mathbf{k}_1) - [\nu_s c_n^2(\mathbf{k}_1) + \nu_h c_n^2(\mathbf{k}_2) \\ &\quad + \nu_h c_n^2(\mathbf{k}_3)]c_n(\mathbf{k}_1), \end{aligned} \tag{35}$$

where ν_s is as defined in Eq. (25) and

$$\nu_h = 4\beta\overline{f}(k_0)[\overline{g}_-(0) + \overline{g}_-(\sqrt{3}k_0) + \beta\overline{f}(k_0)]. \tag{36}$$

The equations for the amplitudes $a_n(\mathbf{k}_2)$ and $a_n(\mathbf{k}_3)$ can be obtained from Eq. (35) by cyclically permuting $\mathbf{k}_1$, $\mathbf{k}_2$, and $\mathbf{k}_3$.

Equation (35) was obtained by making a scaling ansatz for the amplitudes and keeping the lowest order terms. We derive it rigorously using the method of multiple time scales [34] and an averaging procedure in Ref. [33].

If we set $x_n = c_n(\mathbf{k}_1)$, $y_n = c_n(\mathbf{k}_2)$, and $z_n = c_n(\mathbf{k}_3)$, we have

$$\begin{aligned} x_{n+1} &= (1+\epsilon)x_n - (\nu_s x_n^2 + \nu_h y_n^2 + \nu_h z_n^2)x_n, \\ y_{n+1} &= (1+\epsilon)y_n - (\nu_s y_n^2 + \nu_h x_n^2 + \nu_h z_n^2)y_n, \\ z_{n+1} &= (1+\epsilon)z_n - (\nu_s z_n^2 + \nu_h x_n^2 + \nu_h y_n^2)z_n. \end{aligned} \tag{37}$$

If $\nu_s > 0, \nu_s + 2\nu_h > 0$, the amplitudes x_n, y_n and z_n will grow on the slow scale ϵn and then saturate.

We will now determine all the fixed points and their stability. The origin $(x,y,z) = (0,0,0)$ is unstable and has three unstable eigenvalues, all equal to $1+\epsilon$.

The *stripe solutions* are obtained by setting two of the amplitudes, say y_n and z_n equal to zero. This is an invariant manifold for the system. Setting $y_n = 0$ and $z_n = 0$ reduces the system to the case considered in Sec. IX A. A stripe fixed point is given by $x = h_{\rm st}, y = z = 0$. Linearizing Eq. (37) about this fixed point, we obtain

$$\delta x_{n+1}=(1-2\epsilon)\,\delta x_n,$$

$$\delta y_{n+1}=\left(1+\epsilon\frac{\nu_s-\nu_h}{\nu_s}\right)\delta y_n,$$

$$\delta z_{n+1}=\left(1+\epsilon\frac{\nu_s-\nu_h}{\nu_s}\right)\delta z_n.$$

The eigendirection $\delta y_n=\delta z_n=0$ has an eigenvalue $\lambda_s=1-2\epsilon$ and is always stable. The eigendirections $\delta x_n=\delta z_n=0$ and $\delta x_n=\delta y_n=0$ both have the eigenvalue

$$\lambda_1=1+\epsilon\frac{\nu_s-\nu_h}{\nu_s}.$$

Consequently, the stripe solutions are stable if $\nu_h>\nu_s$, and are unstable otherwise.

We can also look at solutions with $x_0=y_0$ and $z_0=0$. These solutions have $x_n=y_n$ and $z_n=0$ for all n, so that the line where $x=y$ and $z=0$ is also an invariant manifold for the system. The evolution of x_n is then given by

$$x_{n+1}=(1+\epsilon)x_n-(\nu_s+\nu_h)x_n^3.$$

Since $\nu_h+\nu_s>0$ from the assumptions that $\nu_s>0$ and $\nu_s+2\nu_h>0$, the amplitudes will grow and saturate at

$$x=y=h_{rh}=\left(\frac{\epsilon}{\nu_s+\nu_h}\right)^{1/2}.$$

Linearizing Eq. (37) about this fixed point, we obtain

$$\delta x_{n+1}=\left(1-\frac{2\nu_s\epsilon}{\nu_s+\nu_h}\right)\delta x_n-\frac{2\nu_h\epsilon}{\nu_s+\nu_h}\,\delta y_n,$$

$$\delta y_{n+1}=\left(1-\frac{2\nu_s\epsilon}{\nu_s+\nu_h}\right)\delta y_n-\frac{2\nu_h\epsilon}{\nu_s+\nu_h}\,\delta x_n,$$

$$\delta z_{n+1}=\left(1+\epsilon\frac{\nu_s-\nu_h}{\nu_s+\nu_h}\right)\delta z_n.$$

Calculating the eigenvalues and the eigenvectors about this fixed point, we see that $\delta x_n=\delta y_n$ and $\delta z_n=0$ are always stable directions, and the corresponding eigenvalues is $\lambda_s=1-2\epsilon$. The directions $\delta x_n=-\delta y_n$ and $\delta z_n=0$ have an eigenvalue

$$\lambda_p=1+2\epsilon\frac{\nu_h-\nu_s}{\nu_s+\nu_h},$$

and the direction $\delta x_n=\delta y_n=0$ has an eigenvalue

$$\lambda_\perp=1+\epsilon\frac{\nu_s-\nu_h}{\nu_s+\nu_h}.$$

Since $\lambda_p>0$ for $\nu_h>\nu_s$ and $\lambda_\perp>0$ for $\nu_s>\nu_h$ generically, there is no range of parameter values for which the rhombus solutions are stable.

If $x_0=y_0=z_0, x_n=y_n=z_n$ for all n, so that the line $x=y=z$ is an invariant manifold for the system. In this case, x_n satisfies

$$x_{n+1}=(1+\epsilon)x_n-(\nu_s+2\nu_h)x_n^3.$$

Since $\nu_s+2\nu_h>0$, the amplitudes will grow and saturate at

$$x=y=z=h_{hx}=\left(\frac{\epsilon}{\nu_s+2\nu_h}\right)^{1/2}.$$

Linearizing Eq. (37) about this fixed point and calculating the eigenvalues and eigenvectors about this fixed point, we see that $\delta x_n=\delta y_n=\delta z_n$ is always a stable direction, and the corresponding eigenvalue is $\lambda_s=1-2\epsilon$. The directions $\delta x_n=-\delta y_n, \delta z_n=0$ and $\delta x_n=-\delta z_n, \delta y_n=0$ both have the same eigenvalue

$$\lambda_2=1+2\epsilon\frac{\nu_h-\nu_s}{\nu_s+2\nu_h}.$$

Therefore, the hexagon solutions are stable when $\nu_s>\nu_h$.

Finally, we can look at the case $\nu_s=\nu_h$. In this case, there is a sphere of fixed points given by

$$x^2+y^2+z^2=\frac{\epsilon}{\nu_s+2\nu_h}.$$

This sphere includes the stripe, rhombus, and hexagon solutions, and it gives continuous families of solutions connecting the various fixed points. The rhombus solutions are generically linearly unstable. The analysis of the bifurcations between the stripe and hexagon solutions is similar to the analysis in Sec. IX B. In particular, the bifurcation between these two patterns occurs at $\nu_s=\nu_h$, and is nonhysteretic. However, since λ_1 and λ_2 tend to zero linearly in $\nu_s-\nu_h$, for runs of finite length T, there will be a region of coexistence in the parameter space, whose width is given by $\Delta p\sim(\epsilon T)^{-1}$.

From the above analysis, we see that the hexagon solution is given by

$$\xi_n(\mathbf{x})=\xi_*+\left[\frac{\beta\overline{f}(k_0)\epsilon}{\nu_s+2\nu_h}+(-1)^n\left(\frac{\epsilon}{\nu_s+2\nu_h}\right)^{1/2}\right]\times[e^{i\mathbf{k}_1\cdot\mathbf{x}}+e^{-i\mathbf{k}_1\cdot\mathbf{x}}+e^{i\mathbf{k}_2\cdot\mathbf{x}}+e^{-i\mathbf{k}_2\cdot\mathbf{x}}+e^{i\mathbf{k}_3\cdot\mathbf{x}}+e^{-i\mathbf{k}_3\cdot\mathbf{x}}]+O(\epsilon). \quad (38)$$

Although we have exhibited an explicit hexagon solution near onset, this is not observed either in the experimental model or in our CCM model. This is a consequence of the fact that the hexagon solution is linearly unstable near the onset of the period-2 patterns. Figure 13 shows ν_h-ν_s at onset ($\epsilon=0$) as a function of k_c/k_0 for our model. ν_h-ν_s is piecewise constant, because of our choice $\phi(k)=\mathrm{sgn}(k_c^2-k^2)$ is a piecewise constant function. Since $\nu_h>\nu_s$ for all $k_c/k_0>1$, it follows that the hexagon solutions are unstable close to onset. (Note that this may not be a universal result since it depends on the details that are specific to our model.)

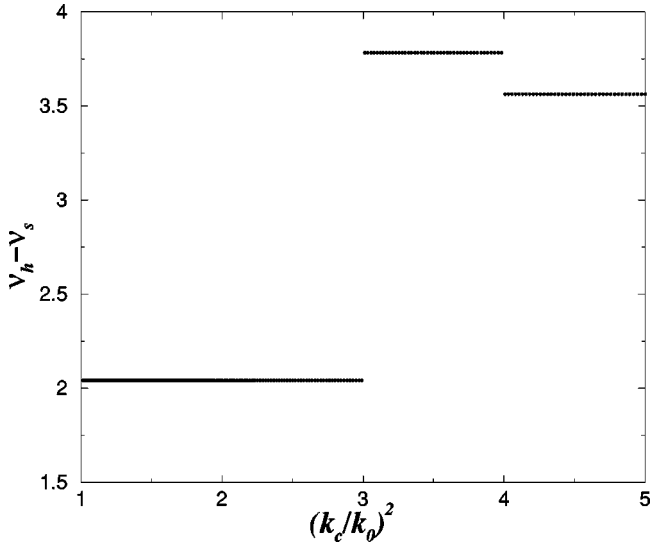

FIG. 13. ν_h-ν_s as a function of k_c/k_0 at onset ($\epsilon=0$).

We expect that hexagons are not observed in the experiments, near the onset of period-2 patterns, for a similar reason.

We will conclude our discussion of the hexagon solution by looking the symmetry properties of these solutions. In the case of one- and two-mode solutions, using the translation invariance of the system, we can always make the mode amplitudes real and positive for even iterations. In contrast, $\mathbf{k}_1+\mathbf{k}_2+\mathbf{k}_3=\mathbf{0}$ implies that the product $a_n(\mathbf{k}_1)a_n(\mathbf{k}_2)a_n(\mathbf{k}_3)$ is invariant under translations. Consequently, unlike in earlier cases, we cannot assume that the amplitudes are real. Also, even if the amplitudes are real, there are two distinct phases corresponding to the case where the product is positive and when the product is negative. The case where the product of the amplitudes is positive corresponds to the peaked phase, where, as viewed from above, the pattern consists of a triangular lattice of peaks. The case where the product of the amplitudes is negative corresponds to the cellular phase, where, as viewed from above, the pattern consists of a honeycomblike structure. These two phases are distinct, and one cannot be obtained from the other by translations, rotations, and reflections in the plane.

D. Two frequency forcing

As we observed in Sec. IX C, hexagons are not observed in the experiment, or in simulations with our model, near the onset of the period-2 patterns. Experimentally, hexagons are observed near the onset of the period-2 patterns, by adding a small subharmonic component with frequency $f_0/2$ to the sinusoidal forcing with frequency f_0 [12], breaking the $1/f_0$ time translation invariance of the dynamics. Also, hexagons are observed in the experiments, and in our simulations, arising as a supercritical bifurcation from the period-2 flat states on decreasing the forcing (Γ in the experiments and r in our simulations, as illustrated, for example in Fig. 4). Thus, it would seem that, breaking the $1/f_0$ (or $n\rightarrow n+1$) time translation symmetry of the system, will increase the stability of the hexagon solutions, thereby making them observable.

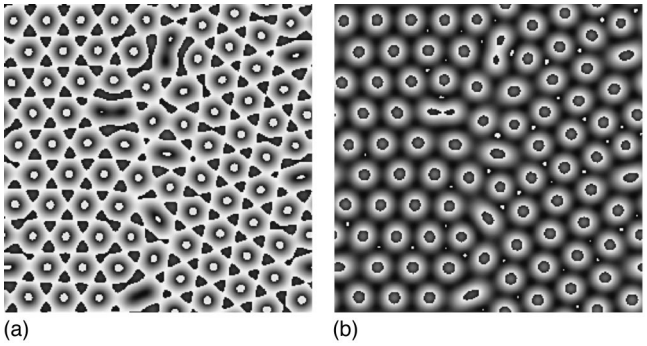

FIG. 14. Hexagonal patterns with two frequency forcing. The parameters are $r=1.7$, $\rho=0.05$, $\rho=2$, and $(k_c/k_0)^2=5.0$.

We can model the effects of adding a subharmonic component to the forcing, by making the parameter r in our model vary periodically with the time index n as

$$r_n = r + (-1)^n \rho. \tag{39}$$

The parameter ρ is a measure of the subharmonic breaking of the $n\rightarrow n+1$ time translation invariance (but still giving an $n\rightarrow n+2$ time translation invariance).

In this section, we will consider the crossover between the behavior of the system with an $n\rightarrow n+1$ time translation invariance, and the behavior with an $n\rightarrow n+2$ but no $n\rightarrow n+1$ time translation invariance. As we discuss in Sec. IX C, the relevant small parameter for the regime with time translation invariance is the supercriticality parameter ϵ. In order to study the crossover behavior, it is useful to have a formulation where we can vary the parameters ϵ and ρ independently, keeping all the other parameters fixed. To achieve this, we modify the definition of our model as

$$\xi_n'(\mathbf{x}) = M[\xi_n(\mathbf{x}), r_n],$$

$$\xi_{n+1}(\mathbf{x}) = \mathcal{L}[\xi_n'(\mathbf{x})], \tag{40}$$

where the nonlinear map M is given by Eq. (5). Note that the time dependence of the quantity r_n, will, in general, break the $n\rightarrow n+1$ time translation symmetry of our model [35]. The linear operator $\mathcal{L}$ is given by Eq. (3), where the spatial Fourier transform of the kernel f is rotationally invariant, and is given by

$$\overline{f}(k) = \exp\left\{\frac{\gamma}{2}\left(\frac{k}{k_0}\right)^2\left[1-\frac{1}{2}\left(\frac{k}{k_0}\right)^2\right]\right\}\mathrm{sgn}(k_c^2-k^2). \tag{41}$$

We have introduced a parameter γ, such that $|\overline{f}(k_0)| = \exp(\gamma/4)$. This is a generalization of the model considered in the preceding sections, which corresponds to setting $\gamma=1$. By varying γ, we can vary $\overline{f}(k_0)$ and consequently vary ϵ, keeping r fixed.

Figure 14 shows the patterns obtained by numerical simulations of the system given by Eqs. (39), (40), (5), (3), and (41), starting from small amplitude random initial conditions. Note that breaking the time translation invariance gives stable hexagon patterns, in a parameter regime where stripes are otherwise stable, as in the experiments [12].

We will now analyze the patterns, in the situation where the time translation invariance is broken. We begin by looking for a stable period-2 orbit for the dynamics

$$\xi_{n+1}=M(\xi_n,r_n),$$

with r_n given by Eq. (39). If $\xi=\xi_*$ is a stable fixed point for the map $M(.,r)$, for sufficiently small ρ, a stable period-2 orbit is given by $\xi_n=\xi_1$ for n odd and $\xi_n=\xi_2$ for n even, with

$$\xi_i=\xi_*-(-1)^i\frac{M_r(\xi_*,r)}{1+\lambda(r)}\rho+O(\rho^2),$$

for $i=1$ and 2, where $M_r(\xi,r)$ is the partial derivative of M with respect to r, and $\lambda(r)=M_\xi(\xi_*,r)$ is as defined in Sec. VIII. We derive this relation in Appendix B [see Eq. (B1)].

A spatially homogeneous solution for the system is therefore given by

$$\xi_n(x)=\frac{\xi_1+\xi_2}{2}+(-1)^n\frac{\xi_2-\xi_1}{2}. \tag{42}$$

We need to consider the linearization about this solution. If $N_1=M_\xi(\xi_1,r-\rho)$ and $N_2=M_\xi(\xi_2,r+\rho)$, as we show in Appendix B [see Eq. (B2)],

$$N_i=\lambda(r)+(-1)^i\left[M_{\xi r}-\frac{M_{\xi\xi}M_r}{1+\lambda(r)}\right]\rho+O(\rho^2),$$

where the partial derivatives are evaluated at (ξ_*,r). The stability index λ_2 is defined by

$$\lambda_2=N_1N_2,$$

and the symmetry breaking parameter Δ is defined by

$$\Delta=\frac{N_2-N_1}{N_1+N_2}.$$

In terms of λ_2 and Δ, we have

$$N_i=(1+(-1)^i\Delta)\left[-\left(\frac{\lambda_2}{1-\Delta^2}\right)^{1/2}\right],$$

for $i=1$ and 2. N_1, $N_2\to\lambda(r)$ as $\Delta\to0$. As we are interested in the parameter regime close to the onset of period-2 patterns, we have to take the negative square root in the above equation, since $\lambda(r)\overline{f}(k_0)=-1$ at onset.

We now consider the evolution of small, spatially varying perturbations, about the spatially homogeneous solutions. The supercriticality parameter ϵ is given by the growth rate of the most unstable modes, so that

$$(1+\epsilon)^2=\lambda_2|\overline{f}(k_0)|^2=\lambda_2\exp(\gamma/2),$$

and varying γ keeping all the other parameters fixed enables us to vary ϵ. The growth rate for the most unstable mode now depends on the time index n, and is given by

$$N_n\overline{f}(k_0)=-[1+(-1)^n\Delta]\frac{1+\epsilon}{\sqrt{1-\Delta^2}}$$

$$=\frac{-(1+\epsilon)}{\sqrt{1-\Delta^2}}-(-1)^n\frac{(1+\epsilon)\Delta}{\sqrt{1-\Delta^2}}. \tag{43}$$

Following a similar procedure to the case of single frequency forcing, one can derive the equations for the mode amplitudes with three dominant modes, for two frequency forcing. Instead of doing this rigorously, we will derive the appropriate equation from symmetry considerations and the requirement that they reduce to the corresponding (known) equations for the case of single frequency forcing as $\Delta\to0$.

As in Sec. IX C, we consider the case with three dominant modes with wave vectors $\mathbf{k}_1$, $\mathbf{k}_2$, and $\mathbf{k}_3$, where $\mathbf{k}_1+\mathbf{k}_2+\mathbf{k}_3=0$ and $|\mathbf{k}_1|=|\mathbf{k}_2|=|\mathbf{k}_3|=0$. The amplitudes of these modes are given by $a_n(\mathbf{k}_i)=d_n(\mathbf{k}_i)+(-1)^nc_n(\mathbf{k}_i)$ for $i=1$, 2, and 3. Using the expression in Eq. (43), and

$$d_{n+1}(\mathbf{k}_i)+(-1)^{n+1}c_{n+1}(\mathbf{k}_i)\approx N_n[d_n(\mathbf{k}_i)+(-1)^nc_n(\mathbf{k}_i)],$$

for the linear growth, we obtain the linearized equations

$$c_{n+1}(\mathbf{k}_i)\approx\frac{(1+\epsilon)}{\sqrt{1-\Delta^2}}c_n(\mathbf{k}_i)+\Delta d_n(\mathbf{k}_1),$$

$$d_{n+1}(\mathbf{k}_1)\approx-\Delta c_n(\mathbf{k}_i)-d_n(\mathbf{k}_1),$$

by expanding and collecting the terms with and without a time dependence of the form $(-1)^n$, and assuming that $|d_n|\ll|c_n|$. The full equation for these amplitudes should be invariant under rotations, and under the transformation

$$\Delta\to-\Delta,c_n(\mathbf{k}_i)\to-c_n(\mathbf{k}_i),d_n(\mathbf{k}_i)\to d_n(\mathbf{k}_i).$$

Also, they should reduce to Eq. (35) as $\Delta\to0$. These requirements significantly constrain the possible forms of the equations governing the evolution of the amplitudes. In particular, the lowest order equations for the dynamics of the amplitudes are given by

$$\begin{aligned}
d_{n+1}(\mathbf{k}_1)&=\beta\overline{f}(k_0)c_n(\mathbf{k}_2)c_n(\mathbf{k}_3)+\nu_e\Delta c_n(\mathbf{k}_1),\\
c_{n+1}(\mathbf{k}_1)&=\frac{(1+\epsilon)}{\sqrt{1-\Delta^2}}c_n(k_1)+\nu_f\Delta d_n(\mathbf{k}_2)\\
&\quad+\nu_g\Delta c_n(\mathbf{k}_2)c_n(\mathbf{k}_3)-[\nu_sc_n^2(\mathbf{k}_1)+\nu_hc_n^2(\mathbf{k}_2)\\
&\quad+\nu_hc_n^2(\mathbf{k}_3)]c_n(\mathbf{k}_1).
\end{aligned} \tag{44}$$

Note that these equations, as well as expressions for ν_f and ν_g, can be obtained by a rigorous derivation through a multiple-scale analysis [33]. The quantities ν_s, ν_h, β, and $\overline{f}(k)$ are as defined earlier. These quantities as well as the quantities ν_e, ν_f, and ν_g depend on the map M, the linear operator $\mathcal{L}$, and the parameter r, but are independent of the parameters ϵ and Δ (more precisely, they have finite nonzero limits as $\epsilon\to0$ and $\Delta\to0$).

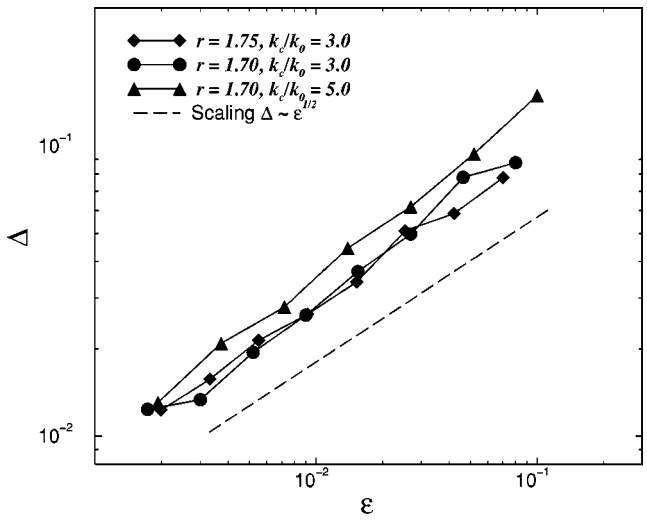

FIG. 15. Crossover between the stripe patterns and the hexagons. The dashed line is the theoretical scaling $\Delta \sim \epsilon^{1/2}$, and the symbols are numerically obtained values of the parameters at the bifurcation between the stripe patterns and the hexagon patterns.

The solutions for the single frequency forcing were obtained by the scaling ansatz $d_n = O(\epsilon)$ and $c_n = O(\sqrt{\epsilon})$. Substituting this ansatz into Eq. (44), we see that this scaling is consistent if $\Delta \ll \sqrt{\epsilon}$. For $\Delta \gg \sqrt{\epsilon}$, consistent scalings are $d_n = O(\Delta^2)$ and $c_n = O(\Delta)$, and there is a crossover between these two scaling regimes when $\Delta \sim \sqrt{\epsilon}$.

In the regime $\epsilon \gg \Delta^2$, the effect of breaking the time translation invariance is negligible, and the behavior of the system is similar to the behavior with $\Delta = 0$. In particular, we do not expect to see stable hexagons in this regime. In contrast, for $\epsilon \ll \Delta^2$, the dynamics is dominated by the effects of the symmetry breaking. In this regime, stable hexagons are observed, as in the experiments [12].

Figure 15 is a numerically obtained bifurcation diagram, for the transition between stripe patterns and hexagons as a function of the supercriticality parameter ϵ and the symmetry breaking parameter Δ. Note that the results are consistent with our prediction that the crossover occurs when $\Delta \sim \epsilon^{1/2}$. In the experiments, if the (nondimensionalized) two frequency driving is given by

$$h(t) = \Gamma \sin(2\pi f_0 t) + \eta \sin(\pi f_0 t),$$

and the onset of period-2 (stripe) patterns is at $\Gamma = \Gamma_*$, we have

$$\Delta \sim \frac{\eta}{\Gamma_*}, \quad \epsilon \sim \Gamma - \Gamma_*.$$

The preceding analysis would predict that the scaling of η at the onset of hexagon patterns with two frequency forcing is

$$\eta \sim (\Gamma - \Gamma_*)^{1/2}.$$

We conclude this section with a discussion of the symmetries of the hexagons that are observed with two frequency forcing. The quantity

$$\chi = \Delta c_n(\mathbf{k}_1) c_n(\mathbf{k}_2) c_n(\mathbf{k}_3)$$

is invariant under the transformation $\Delta \to -\Delta$, $c_n(\mathbf{k}_i) \to -c_n(\mathbf{k}_i)$, $d_n(\mathbf{k}_i) \to d_n(\mathbf{k}_i)$, which is a symmetry for the dynamical equations. Consequently, there are no symmetry requirements forcing $\langle \chi \rangle$ to be zero, where $\langle \chi \rangle$ is the average value of χ over all the stable solutions for a given set of parameters. This is in contrast to the case of the hexagons with a single frequency forcing, where symmetry requirements imply that both the peaked and the cellular phases are equally likely to be observed at any given time index n, since the average value of the product $c_n(\mathbf{k}_1) c_n(\mathbf{k}_2) c_n(\mathbf{k}_3)$ has to be zero by the time translation invariance. If $\langle \chi \rangle$ is nonzero, we could be in a regime where one kind of hexagonal pattern (say peaked on odd oscillations) is stable while the other kind (in this case, peaked on even cycles) is unstable. In our simulations, we are always in this regime, and we have $\langle \chi \rangle < 0$, so that the peaked phase occurs after the iteration with the larger value of $|N|$, that is, the larger growth rate.

E. Fronts and localized patterns

Let $P(\mathbf{x},n)$ be an asymptotic stable ''global'' pattern for the dynamics in a certain parameter regime, and let $\mathcal{S}$ be the set of all the solutions $\xi_n(\mathbf{x})$ that are equivalent to P modulo the symmetries of the system. If $\mathcal{P}$ is the transformation group of $\mathcal{S}$, as we discuss in Sec. VIII, $\mathcal{P}$ is a subgroup of $\mathcal{G} = \mathbb{Z} \times \mathbb{R}^2 \times O(2)$, the symmetry group for the equations governing the dynamics. Since $\mathbb{Z}$ is a discrete group, $\mathcal{G}$ is not connected. Consequently, $\mathcal{P}$ is not necessarily connected either.

As we argue in Sec. VIII, for long times, the solution $\xi_n(\mathbf{x})$ is given by

$$\xi_n(\mathbf{x}) \approx S_{\tilde{g}(\mathbf{x},n)}[P],$$

where S_g is the action of $g \in \mathcal{P}$ on the pattern P, and $\tilde{g}(\mathbf{x},n) \in \mathcal{P}$ is the field of the local degrees of freedom, that varies only on time scales $T \gg \tau$, and, away from the domain walls, on length scales $l \gg k_0$.

We first consider the case that $\mathcal{P}$ is connected. For any initial configuration of the local degrees of freedom, it is possible to have $\tilde{g}(\mathbf{x},n) \to g_*$ for all $\mathbf{x}$ as $n \to \infty$ in a continuous fashion [36]. In this setting, we expect that the domains will coarsen with some domains growing at the expense of the others, until, the patterns asymptotically converges to a global pattern $S_{g_*}[P]$ on the entire domain.

We will now consider the case in which $\mathcal{P}$ is not connected. Since the local degrees of freedom change continuously on each domain, for all $\mathbf{x}$ in a domain D, $\tilde{g}(\mathbf{x},n)$ is in the same component of $\mathcal{P}$. We consider an initial configuration where $\tilde{g}(\mathbf{x}_1,0)$ and $\tilde{g}(\mathbf{x}_2,0)$ are in different components of $\mathcal{P}$ for points in two different domains D_1 and D_2. We also assume that the domains D_1 and D_2 are large and therefore contain many points that are at distances $l \gg k_0$ from the domain boundaries. In this situation, if the stable pattern P is attracting, for sufficiently large domains the dynamics in the interior of the domain is unaffected by the other domains, and the local degrees of freedom in the interior will not vary

significantly over time. In particular, they always remain in a single component of $\mathcal{P}$. We call the boundary separating two domains a *front*, as the patterns on either side of the boundary correspond to different components of $\mathcal{P}$.

From our discussion of the symmetries of the various, period-2 patterned states near onset, we see that any stripe (square) solution can be obtained from any other stripe (square) solution by appropriate translations and rotations without any time translations or spatial reflections. Since rotations and translations generate continuous groups, $\mathcal{P}$ is connected for these solutions, and fronts do not occur in the period-2 stripes and squares near onset. Although there may be domains of different stripe orientation in the intermediate regime, we do not have fronts, since $\mathcal{P}$ consists of a single component for these patterns. It is observed, both in experiments and simulations, that the solution asymptotically converges to a ''global'' stable pattern, that is a pattern where the orientations are lined up on the entire region.

For hexagon solutions, the peaked phase cannot be transformed into a cellular phase by translations or rotations, and one needs a time translation to generate the set of all the transformations between equivalent hexagon solutions. Thus the transformation group for the period-2 hexagon solutions, with single frequency forcing, is disconnected, and consists of two components. This is also true for stable period-2 homogeneous solutions, which are invariant under time translation by two units but not under time translations by one unit, so that $\mathcal{P}$ is a disconnected group with two elements. Thus we expect to see two distinct domains and fronts separating these domains, both in the hexagon solutions with single frequency forcing and in the period-2 homogeneous solutions. These fronts are indeed observed in the experiments [10,12], as well as our numerical simulations (see Fig. 3).

For the case of the two frequency forcing, the dynamics is not invariant under translations by one time step. It is, however, invariant under translations by two time steps. As we discuss in Sec. IX D, in our simulations stable hexagons are observed in a regime where only one type of hexagon solution is stable. We can show that, for this case, the transformation group $\mathcal{P}$ is connected. This is reflected in our numerical simulations with two frequency forcing, where we do not observe fronts. This is also true in the experiments with two frequency forcing [12].

An implicit assumption underlying our discussion of pattern selection has been that there is a unique stable attracting pattern P for a given set of parameters in the sense that any two ''global'' asymptotic stable solutions are related by a symmetry transformation in $\mathcal{P}\subseteq\mathcal{G}$. This assumption is justified by our analysis of the various patterns in Sec. VII and Secs. IX A–IX C, wherein we observe that all transitions between the various patterned states, as well as the onset of the patterned states, are nonhysteretic. A necessary condition for this to be true is that the period doubling bifurcations of the map M should be supercritical. If the period doubling is subcritical, there exist parameter regimes with multiple stable patterns, and new phenomena are observed in these regimes. In particular, with the map in Eq. (9) used in place of the map in Eq. (5), there is a parameter regime where period-2 squares and the period-1 homogeneous state are both linearly stable. In this regime, as depicted in Fig. 6, we observe localized, period-2 structures on a homogeneous period-1 background, that are similar to the oscillons seen in the experiments [11,12]. These localized structures are distinct from the fronts and domains that we discussed earlier, in that, the size of these localized structures is of the order of k_0^{-1}, unlike the domains in patterns with fronts, which had to be of a size $l \gg k_0^{-1}$. These states cannot be analyzed using the weakly nonlinear analysis, of Secs. IX A–IX D, since the oscillon states do not evolve continuously from a homogeneous state as a parameter is varied. An analysis of these structures may require a new set of ideas, and it presents a very interesting theoretical challenge.

X. DISCUSSION

The spirit of our model is similar to that of other generic models of spatiotemporal dynamics [1], and may be regarded as lying between continuous time–continuous space models (e.g., the Swift-Hohenberg and the complex Ginzburg-Landau equations) and coupled map lattice models [37,38]. Our approach of choosing a discrete time and a continuous spatial domain, is motivated by the symmetries of a periodically forced extended system, namely, a discrete time translation symmetry and a continuous symmetry under spatial translations and rotations. In the context of models for vibrated sand experiments, CCM models provide the simplest possible description of temporal period doubling, while allowing for spatial patterns unconstrained by an imposed grid [39].

While we have not incorporated any physics specific to granular materials in the construction of our model, the model captures many features of the bifurcations that are observed experimentally. Further, analysis implies that these features do not depend sensitively on the exact choices we make for the functions $M(\xi,r)$ and $\overline{f}(\mathbf{k})$ that define our model. In this sense, these bifurcation phenomena may be regarded as universal to the class of systems with the following features.

(1) The system is strongly dissipative, and it can be effectively described by one scalar field ξ.

(2) The interactions are not long ranged, and it is meaningful to talk about a ''local'' temporal dynamics for $\xi(\mathbf{x})$ at any given location x.

(3) The ''local'' temporal dynamics undergoes period doubling bifurcations as the parameters are varied.

(4) There is pattern formation at a preferred length scale.

Our approach then enables us to study the effects of additional physical considerations, like the presence of a second length scale (this generically leads to the formation of square patterns), breaking the $t \to t+1/f_0$ time translation symmetry (this leads to the stabilization of hexagonal patterns) and the effects of hysteresis (this leads to the formation of oscillons and other localized structures), and these can be regarded as universal properties of systems with these features. In particular, we would also expect to see these phenomena in other systems besides vibrated granular material.

Note that our framework for a CCM model separates the temporal dynamics [Eq. (1)] and the spatial coupling [Eq. (2)]. Furthermore, the spatial coupling operator is linear. Thus our framework for the CCM model has a special structure that is not, in general, present in physical situations. However, the individual qualitative spatiotemporal bifurcations we find are generic in that they persist under small changes of the system, e.g., changes that ''mix'' the temporal and the spatial dynamics.

As a second point, we note that a designation of a phenomenon as ''generic'' or ''universal'' does not imply that it always occurs [e.g., for a smooth map $M(x,r)$, a single period doubling does not necessarily guarantee the occurrence of a full period doubling cascade]. For example, in the case of Faraday waves on a vertically vibrated fluid layer, a period doubled homogeneous state is ruled out by incompressibility. Thus, when we label a phenomenon as generic or universal, we only require that the phenomenon persist under small changes of the system (or equivalently the model equations) and not that the phenomena always occur. As an illustration, for the case of vibrated granular materials, different choices of M and $\mathcal{L}$ in Eqs. (1) and (2) may produce phase diagrams that differ somewhat from Fig. 4.

Finally we wish to emphasize that our model is constructed so that it is simple. As we pointed out earlier, it can be generalized in may ways. While our model gives good qualitative agreement with experiments on vibrated granular layers, there are certain features of the experiment that cannot be captured by our model due to its simplicity. We have chosen a scalar field variable ξ representing the height of the granular layer to describe the state of the system. However, one would expect that the physics of the experimental system depends both on the height of the layer, as well as the location of the bottom of the layer relative to the oscillating plate. In particular, our model cannot distinguish between the behaviors represented in Figs. 2(b) and 2(c), and both these behaviors appear as period-2 cycles of the map. We therefore lose the information that the bottom of the layer hits the plate only once every two cycles in Fig. 2(c), unlike in Fig. 2(b), where the bottom hits the plate on every cycle. In experiments [10–12], the transition form period-2 patterns to period-2 flat states on increasing Γ apparently coincides with the onset of the layer behavior as in Fig. 2(c), i.e., the layer makes contact with the plate once every two oscillation cycles. If we do the analogous numerical simulation with our model, namely, we follow a solutions by varying the parameter r, then the period-2 patterns do not disappear on increasing r. Consequently, the transitions between the period-2 patterns and the period-2 flat state in our model shows substantial hysteresis unlike in the experiment. In particular, the phase diagram (Fig. 4) is obtained by starting with a random initial condition that is close to a homogeneous state, and not by following solutions by continuously varying the parameters r and k_c/k_0.

This discussion would suggest that we can improve the agreement between our model and the experiment by considering two scalar fields $\xi(\mathbf{x})$ and $\eta(\mathbf{x})$ representing the top and the bottom of the granular layer, using a two-dimensional map $(\xi_{n+1},\eta_{n+1})=\mathbf{M}(\xi_n,\eta_n,r)$ instead of the one-dimensional map in Eq. (5), and appropriately modifying the spatial coupling to account for the presence of two fields. We have refrained from doing this, since this would make the model considerably more complex. It would also give us a larger number of undetermined parameters in the maps and in the couplings. While this might yield better agreement with the experiments by making proper choices, it runs counter to our basic approach, which has been to find a simple model that explains the dynamical underpinnings of the observed phenomena, that are independent of physics specific to granular materials. Thus we wish to emphasize that our particular model does not probe the details of the physics of granular materials, but is geared toward finding the universal features of systems where pattern formation and temporal period doubling interact.

In conclusion, we believe that the CCM approach will be fruitful in the investigation of other systems beside vibrated granular layers. In this paper, we present a framework for the construction of a CCM model, given certain basic physical considerations, like dimensional analysis and the symmetries underlying the system. We also give a procedure for the analysis of these models, using truncated modal expansions and the separation of the time scales in the dynamics. This approach can be extended to other periodically forced extended systems. In particular, this approach might yield useful results in the study of forced, strongly dissipative extended systems, e.g., the experiments on vibrated layers of very viscous fluids [40].

ACKNOWLEDGMENTS

We thank Chris Bizon, Greg Huber, Heinrich Jaeger, Markus Löcher, Mark Shattuck, Harry Swinney, and Paul Umbanhowar for valuable discussions. S. C. V. acknowledges support from the Alfred P. Sloan Jr. Foundation and by the National Science Foundation under Award No. DMR 9975533. The work of E.O. was supported by the Office of Naval Research (Physics).

APPENDIX A: THREE DOMINANT MODES

In the case with three dominant modes, $C_2=\{\mathbf{0},\pm2\mathbf{k}_1,\pm2\mathbf{k}_2,\pm2\mathbf{k}_3,\pm(\mathbf{k}_1-\mathbf{k}_2),\pm(\mathbf{k}_2-\mathbf{k}_3),\pm(\mathbf{k}_3-\mathbf{k}_1)\}$. Eq. (21) yields the following expressions for the mode amplitudes:

$$\begin{aligned}
d_n(\mathbf{0}) &= 2\overline{g}_-(0)[|c_n(\mathbf{k}_1)|^2+|c_n(\mathbf{k}_2)|^2+|c_n(\mathbf{k}_3)|^2 \\
&\quad +|d_n(\mathbf{k}_1)|^2+|d_n(\mathbf{k}_2)|^2+|d_n(\mathbf{k}_3)|^2],\\
c_n(\mathbf{0}) &= 2\overline{g}_+(0)[c_n(\mathbf{k}_1)d_n^*(\mathbf{k}_1)+c_n(\mathbf{k}_2)d_n^*(\mathbf{k}_2) \\
&\quad +c_n(\mathbf{k}_3)d_n^*(\mathbf{k}_3)+d_n(\mathbf{k}_1)c_n^*(\mathbf{k}_1)+d_n(\mathbf{k}_2)c_n^*(\mathbf{k}_2) \\
&\quad +d_n(\mathbf{k}_3)c_n^*(\mathbf{k}_3)],\\
d_n(\mathbf{k}_1-\mathbf{k}_2) &= \overline{g}_-(\sqrt{3}k_0)[c_n(\mathbf{k}_1)c_n^*(\mathbf{k}_2)+d_n(\mathbf{k}_1)d_n^*(\mathbf{k}_2)],\\
c_n(\mathbf{k}_1-\mathbf{k}_2) &= \overline{g}_+(\sqrt{3}k_0)[c_n(\mathbf{k}_1)d_n^*(\mathbf{k}_2)+d_n(\mathbf{k}_1)c_n^*(\mathbf{k}_2)],\\
d_n(2\mathbf{k}_1) &= \overline{g}_-(2k_0)[c_n^2(\mathbf{k}_1)+d_n^2(\mathbf{k}_1)]
\end{aligned} \tag{A1}$$

$$c_n(2\mathbf{k}_1) = 2\overline{g}_+(2k_0)c_n(\mathbf{k}_1)d_n(\mathbf{k}_1).$$

The mode amplitudes for all the modes in C_2 can be obtained from the above expressions by complex conjugation and cyclic permutation.

APPENDIX B: PERIOD-2 FORCING FOR THE MAP

We consider the dynamical system

$$\xi_{n+1} = M(\xi_n, r_n),$$

where

$$r_n = r + (-1)^n \rho,$$

r is such that $\xi = \xi_*$ is a stable fixed point for the map $M(.,r)$ and ρ is small, i.e.,

$$|M_{\xi r}(\xi^*, r)\rho| \ll 1 - |\lambda(r)|.$$

We have used subscripts to denote partial derivatives, and $\lambda(r) = M_\xi(\xi^*, r)$ is the stability index of the fixed point for the map $M(.,r)$. We have a period-2 orbit $\xi_n = \xi_1$ for n odd and $\xi_n = \xi_2$ for n even if we have a solution to

$$\xi = M[M(\xi, r-\rho), r+\rho].$$

The solution to this equation gives the value ξ_n for the odd iterates. $\xi = \xi^*$ is a solution for $\rho = 0$. Using the implicit function theorem, we will show that there is a solution close to $\xi = \xi^*$ for sufficiently small ρ. Assuming the existence of a solution $\xi(\rho)$, we can differentiate the above expression to obtain

$$\frac{d\xi}{d\rho} = M_\xi[M(\xi, r-\rho), r+\rho]\left(M_\xi(\xi, r-\rho)\frac{d\xi}{d\rho} - M_r(\xi, r-\rho)\right) + M_r[M(\xi, r-\rho), r+\rho].$$

Rearranging, we obtain

$$\frac{d\xi}{d\rho} = \frac{M_r[M(\xi, r-\rho), r+\rho] - M_\xi[M(\xi, r-\rho), r+\rho]M_r(\xi, r-\rho)}{1 - M_\xi[M(\xi, r-\rho), r+\rho]M_\xi(\xi, r-\rho)}.$$

At $\rho = 0, \xi = \xi^*$, we have $M_\xi(\xi^*, r) = \lambda(r)$. The above expression then simplifies to give

$$\frac{d\xi}{d\rho} = \frac{M_r(\xi^*, r)}{1 + \lambda(r)}.$$

Since the fixed point ξ^* is stable, $|\lambda(r)| < 1$, so that the implicit function theorem applies and we have that, for $i = 1$ and 2, and for sufficiently small ρ,

$$\xi_i = \xi_* - (-1)^i \frac{M_r(\xi_*, r)}{1 + \lambda(r)}\rho + O(\rho^2). \tag{B1}$$

We now consider the stability of this solution. If $N_1 = M_\xi(\xi_1, r-\rho)$ and $N_2 = M_\xi(\xi_2, r+\rho)$, we have

$$N_i = M_\xi[\xi_i, r + (-1)^i\rho] = \lambda(r) + M_{\xi r}(\xi^*, r)\rho + M_{\xi\xi}\frac{d\xi_i}{d\rho}\rho + O(\rho^2)$$

$$= \lambda(r) + (-1)^i\left[M_{\xi r} - \frac{M_{\xi\xi}M_r}{1 + \lambda(r)}\right]\rho + O(\rho^2). \tag{B2}$$

Therefore, $|N_1 N_2| \leqslant \lambda(r)^2 < 1$ if ρ is sufficiently small, so that the period-2 orbit is stable.

[1] M. C. Cross and P. C. Hohenberg, Rev. Mod. Phys. **65**, 851 (1993).

[2] J. P. Gollub and J. S. Langer, Rev. Mod. Phys. **71**, S396 (1999).

[3] A. M. Turing, Philos. Trans. R. Soc. London, Ser. B **327**, 37 (1952); G. Nicolis and I. Prigogine, *Self-Organization in Non-Equilibrium Chemical Systems* (Wiley, New York, 1977); K. J. Lee, W. D. McCormick, H. L. Swinney, and J. E. Pearson, Nature (London) **369**, 215 (1994).

[4] M. Faraday, Philos. Trans. R. Soc. London **121**, 319 (1831); B. Christiansen, P. Alstrom, and M. T. Levinson, Phys. Rev. Lett. **68**, 2157 (1992); A. Kudrolli and J. P. Gollub, Physica D **97**, 133 (1996); D. Binks and W. van de Water, Phys. Rev. Lett. **78**, 4043 (1997).

[5] H. Bénard, Ann. Chim. Phys. **23**, 62 (1901); Lord Rayleigh, Philos. Mag. **32**, 529 (1916); S. Chandrasekhar, *Hydrodynamic and Hydromagnetic Stability* (Oxford University Press, London, 1961); J. B. Swift and P. C. Hohenberg, Phys. Rev. A **15**, 319 (1977); A. V. Getling, *Rayleigh-Bénard Convection: Structures and Dynamics* (World Scientific, Singapore, 1998); E. Bodenschatz, W. Pesch, and G. Ahlers, Annu. Rev. Fluid Mech. **32**, 709 (2000).

[6] A. T. Winfree, Int. J. Bifurcation Chaos Appl. Sci. Eng. **7**, 487 (1997). This article also contains an extensive list of references.
[7] T. Shinbrot and J. M. Ottino, Int. J. Bifurcation Chaos Appl. Sci. Eng. **5**, 955 (1995).
[8] C. Diks, F. Takens, and J. DeGoede, Physica D **104**, 269 (1997).
[9] A. Lemaître and H. Chaté, Phys. Rev. Lett. **82**, 1140 (1999); J. Stat. Phys. **96**, 915 (1999).
[10] F. Melo, P. B. Umbanhowar, and H. L. Swinney, Phys. Rev. Lett. **75**, 3838 (1995).
[11] P. B. Umbanhowar, F. Melo, and H. L. Swinney, Nature (London) **382**, 793 (1996).
[12] P. B. Umbanhowar, F. Melo, and H. L. Swinney, Physica A **249**, 1 (1998).
[13] For other experiments exhibiting phenomena in vertically vibrated granular layers, see T. Metcalf, J. B. Knight, and H. M. Jaeger, Physica A **236**, 202 (1997); F. Melo, P. B. Umbanhowar and H. L. Swinney, Phys. Rev. Lett. **72**, 172 (1994); H. K. Pak and R. P. Behringer, Phys. Rev. Lett. **71**, 1832 (1993); C. Larouche, S. Douady, and S. Fauve, J. Phys. (France) **50**, 699 (1989).
[14] T. Benjamin and F. Ursell, Proc. R. Soc. London, Ser. A **225**, 505 (1954).
[15] K. Kumar and L. Tuckerman, J. Fluid Mech. **279**, 49 (1994); K. Kumar, Proc. R. Soc. London, Ser. A **452**, 1113 (1996); E. Cerda and E. Tirapegui, Phys. Rev. Lett. **78**, 859 (1997).
[16] H. Müller, Phys. Rev. E **49**, 1273 (1994); W. Zhang and J. Viñals, J. Fluid Mech. **336**, 301 (1997); P. Chen and J. Viñals, Phys. Rev. E **60**, 559 (1999).
[17] H. M. Jaeger, S. R. Nagel, and R. P. Behringer, Rev. Mod. Phys. **68**, 1259 (1996).
[18] L. P. Kadanoff, Rev. Mod. Phys. **71**, 435 (1999).
[19] C. Bizon *et al.*, Phys. Rev. Lett. **80**, 57 (1998); J. Stat. Phys. **93**, 449 (1998).
[20] C. K. K. Lun, S. B. Savage, D. J. Jeffery, and N. Chepurniy, J. Fluid Mech. **140**, 223 (1983); J. T. Jenkins and M. W. Richman, Arch. Ration. Mech. Anal. **87**, 355 (1985); J. T. Jenkins and M. W. Richman, Phys. Fluids **28**, 3485 (1985).
[21] J. R. de Bruyn, C. Bizon, M. D. Shattuck, D. Goldman, J. B. Swift, and H. L. Swinney, Phys. Rev. Lett. **81**, 1421 (1998).
[22] C. Bizon, M. D. Shattuck, J. B. Swift, and H. L. Swinney, Phys. Rev. E **60**, 4340 (1999); M. D. Shattuck, C. Bizon, J. B. Swift, and H. L. Swinney, Physica A **274**, 158 (1999); C. Bizon, M. D. Shattuck, and J. B. Swift, Phys. Rev. E **60**, 7210 (1999).
[23] L. S. Tsimring and I. S. Aronson, Phys. Rev. Lett. **79**, 213 (1997).
[24] T. Shinbrot, Nature (London) **389**, 574 (1997).
[25] E. Cerda, F. Melo, and S. Rica, Phys. Rev. Lett. **79**, 4570 (1997).
[26] D. Rothman, Phys. Rev. E **57**, R1239 (1998).
[27] J. Eggers and H. Riecke, Phys. Rev. E **59**, 4476 (1999).
[28] C. Crawford and H. Riecke, Physica D **129**, 83 (1999).
[29] S. C. Venkataramani and E. Ott, Phys. Rev. Lett. **80**, 3495 (1998).
[30] A. Mehta and J. M. Luck, Phys. Rev. Lett. **65**, 393 (1990).
[31] R. Lifshitz and D. M. Petrich, Phys. Rev. Lett. **79**, 1261 (1997). The authors modified the Swift-Hohenberg equation by introducing a second length scale, and this led to patterns besides stripes.
[32] M. Golubitsky, I. N. Stewart and D. G. Schaeffer, *Singularities and Groups in Bifurcation Theory* (Springer-Verlag, New York, 1988), Vol. II.
[33] S. C. Venkataramani and E. Ott (unpublished).
[34] E. J. Hinch, *Perturbation Methods* (Cambridge University Press, Cambridge, 1991); R. E. O'Malley Jr., *Introduction to Singular Perturbations* (Academic Press, New York, 1974).
[35] We do not have to restrict r_n to be time periodic. In particular, we can let r_n be a chaotic sequence or a random sequence. In certain parameter regimes varying r_n irregularly gives states that intermittently switch between stripe patterns and hexagon patterns [Markus Löcher (private communication)].
[36] Since the time index n is a discrete variable, it is incorrect to say that $\tilde{g}(\mathbf{x},n)\rightarrow g_*$ continuously. However, $\tilde{g}$ varies on a scale $T\gg 1$, and by appropriate coarse graining on a scale T we can define a function $g_c(\mathbf{x},t)$ for a continuous variable $t \approx n/T$, such that $\tilde{g}(\mathbf{x},n)=g_c(\mathbf{x},n/T)$. By the statement $\tilde{g}(\mathbf{x},n)\rightarrow g_*$, in a continuous fashion, we mean that the coarse graining yields a continuous, slowly varying, function $g_c(\mathbf{x},t)$ such that $g_c(\mathbf{x},t)\rightarrow g_*$ as $t\rightarrow\infty$.
[37] See, e.g., K. Kaneko, Chaos **2**, 279 (1992). This issue of Chaos focuses on the subject of coupled map lattices.
[38] Another in between case is provided by coupled ordinary differential equations on a spatial lattice; see, e.g., D. K. Umberger, C. Grebogi, E. Ott, and B. Afeyan, Phys. Rev. A **39**, 4835 (1989).
[39] In our numerical solutions of the model [Eqs. (1)–(8)], a spatial grid is used, but the spacing between the grid points is small compared to the characteristic scale k_0^{-1}.
[40] O. Lioubashevski, H. Arbell, and J. Fineberg, Phys. Rev. Lett. **76**, 3959 (1996); J. Fineberg and O. Lioubashevski, Physica A **249**, 10 (1998); O. Lioubashevski, Y. Hamiel, A. Agnon, Z. Reches, and J. Fineberg, Phys. Rev. Lett. **83**, 3190 (1999).